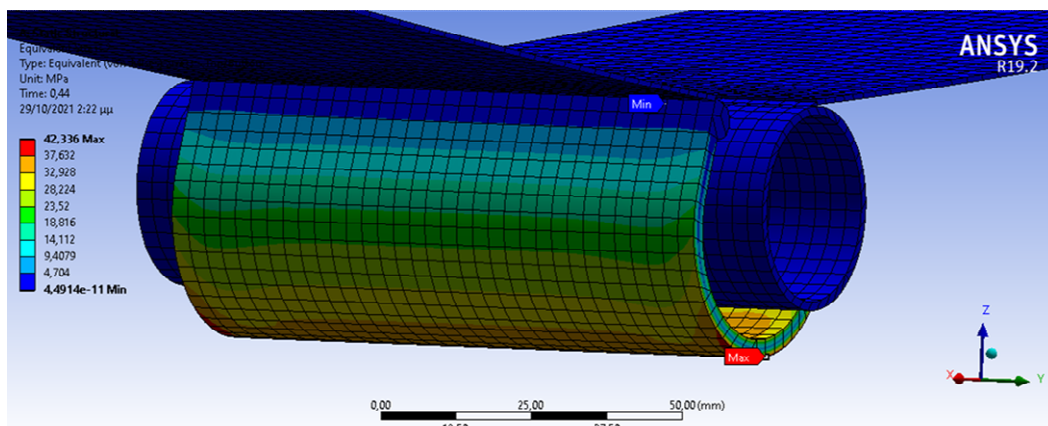




Institute of Steel Structures
School of Civil Engineering
National Technical University of Athens

Design optimization of steel structures for nethouse systems



Master Thesis

Mantas P. Konstantinos

Supervisor

Ioannis Vayas, Professor N.T.U.A.

EMK ME 2021/11

Athens, October 2021

Mantas P.K. (2021).

Design optimization of steel structures for nethouse systems

Master Thesis EMK ME 2021/11

Institute of Steel Structures, National Technical University of Athens, Greece

Μαντάς Π.Κ. (2021).

Βελτιστοποίηση Σχεδιασμού Μεταλλικών Κατασκευών Διχτυοκηπίων

Διπλωματική Μεταπτυχιακή Εργασία EMK ME 2021/11

Εργαστήριο Μεταλλικών Κατασκευών, Εθνικό Μετσόβιο Πολυτεχνείο, Αθήνα

NATIONAL TECHNICAL UNIVERSITY OF ATHENS

FACULTY OF CIVIL ENGINEERING

INSTITUTE OF STEEL STRUCTURES

DIPLOMA THESIS

EMK ME 2021/11

Design optimization of steel structures for nethouse systems

Mantas P. K.

(supervised by Vayas I.)

Abstract

This research work investigates an integrated design methodology for nethouse systems that incorporates an innovative overload release mechanism. Nethouses are lightweight steel structures that intend to protect the high value horticultural production against climatic actions. Up to now, they are not designed for snow loads and as a result their use is either restricted or unsafe. The static behavior of tensile nethouse structures is investigated and through a holistic parametric and comparative analysis the influence of each structural design parameter (cable prestressing, inclination of cables) is indicated.

In addition, nethouse under snow loads, without being supported by an expensive structural system should be designed with an innovative overload release mechanism to get rid of the sudden overload with safety. The conceptual design of the release mechanism is given and numerical models of gradual complexity are developed to predict the load level of the release, examining several geometrical configuration of its components.

ΕΘΝΙΚΟ ΜΕΤΣΟΒΙΟ ΠΟΛΥΤΕΧΝΕΙΟ
ΣΧΟΛΗ ΠΟΛΙΤΙΚΩΝ ΜΗΧΑΝΙΚΩΝ
ΕΡΓΑΣΤΗΡΙΟ ΜΕΤΑΛΛΙΚΩΝ ΚΑΤΑΣΚΕΥΩΝ

ΔΙΠΛΩΜΑΤΙΚΗ ΕΡΓΑΣΙΑ

ΕΜΚ ΜΕ 2021/11

Βέλτιστος σχεδιασμός μεταλλικών κατασκευών διχτυοκηπίων

Μαντάς Π. Κωνσταντίνος,
(επιβλέπων Βάγιας Ι.)

Abstract

Αυτή η ερευνητική εργασία διερευνά μια ολοκληρωμένη μεθοδολογία σχεδιασμού για συστήματα διχτυοκηπίων που ενσωματώνουν έναν καινοτόμο μηχανισμό απελευθέρωσης. Τα διχτυοκήπια είναι ελαφριές κατασκευές από χάλυβα που στόχο έχουν να προστατεύσουν την κηπευτική παραγωγή υψηλής αξίας από τις κλιματικές επιδράσεις. Μέχρι στιγμής, δεν σχεδιάζονται για φορτία χιονιού και ως εκ τούτου η χρήση τους είναι είτε περιορισμένη είτε μη ασφαλής. Διερευνάται η στατική συμπεριφορά των εφελκόμενων συστημάτων διχτυοκηπίων και μέσω μιας ολιστικής παραμετρικής και συγκριτικής ανάλυσης υποδεικνύεται η επίδραση κάθε παραμέτρου σχεδιασμού.

Επιπλέον, το διχτυοκήπιο κάτω από φορτία χιονιού, χωρίς να υποστηρίζεται από ένα στιβαρό δομικό σύστημα θα πρέπει να σχεδιαστεί με έναν καινοτόμο μηχανισμό απελευθέρωσης υπερφόρτωσης για να απαλλαγθεί από την ξαφνική υπερφόρτωση με ασφάλεια. Δίνεται ο εννοιολογικός σχεδιασμός του μηχανισμού απελευθέρωσης και αναπτύσσονται αριθμητικά μοντέλα σταδιακής πολυπλοκότητας για την πρόβλεψη του επιπέδου φορτίου της απελευθέρωσης

CONTENTS

1	Nethouses	7
1.1	General.....	7
1.2	Structural systems.....	8
1.2.1	Framed Structures.....	8
1.2.2	Arched Structures.....	9
1.2.3	Tensile Structures.....	9
1.3	Comparison of the structural systems.....	11
2	Materials	13
2.1	Net.....	13
2.2	Cables.....	14
3	Structural analysis	18
3.1	Methodology.....	18
3.2	Structural Model.....	20
3.3	Investigation of nonlinearity.....	23
3.4	Influence of the anchor angle θ	25
3.5	Influence of prestressing.....	27
3.6	Influence of imperfections.....	29
3.7	Sub-model of membrane.....	30
3.8	Aggregate results.....	35
4	Description of the release mechanism	36
4.1	The necessity of the release mechanism.....	36
4.2	Requirements of the release mechanism.....	37
4.3	Specifications.....	37
5	The operation of release mechanism	39
5.1	The capacity of the mechanism.....	39
5.2	Simply Supported Model.....	41
5.3	Contact supported Model.....	46
5.4	Von mises Stresses of the clip.....	52
5.5	Comparison of models.....	53
6	Further Investigation	58
6.1	Full scale experiment.....	58
6.2	Deformed shape of roof-Ponding.....	62
7	References	64
8	Annex A/ Primary experiments of release mechanism	65

Ευχαριστίες

Ευχαριστώ πολύ τον κύριο Ιωάννη Βάγια, καθηγητή ΕΜΠ που μου έδωσε την ευκαιρία να ασχοληθώ με ένα τόσο ενδιαφέρον θέμα με ερευνητικές προεκτάσεις.

Ευχαριστώ τους ερευνητές κ. Κωνσταντίνο Αδαμάκο και Αναστάσιο Γιαννούλη για την καλή συνεργασία μας.

Ευχαριστώ τον κύριο Δ.Μπριασούλη, καθηγητή ΓΠΑ για τις χρήσιμες συμβουλές του.

Τιμώ όσους με στηρίζουν

Τιμώ όσους με δίδαξαν

1 Nethouses

1.1 General

The nethouses are lightweight structures that intent to protect the high value horticultural production against climatic hazards. They constitute an alternative solution for the greenhouses primarily in hot and sunny regions. Agricultural permeable nets are used as cladding material providing natural protection to crops. The geometric configuration varies (flat, duopitch, arch, gothic) and depends on the prevailing weather conditions of the installation area. By now, there is no European or International design Standards for nethouses and they are constructed following empirical procedures. In particular, the weakness of design standards focuses on determining wind pressures on a permeable structure such as a nethouse as well as the lack of commentary on the inability of such structures to carry significant snow loads. As a result, the majority of the installed nethouses are either unsafe or overdesigned structures. It is worth noting that there is the European Standard EN-13031-1 which guides only the construction of greenhouses with direct references to Eurocode 1 and Eurocode 3, for the determination of the imposed actions and the design of the steel supporting structure, respectively. This study aims to investigate the ability of the nethouses to be installed in areas where significant snow loads are forecast.



Figure 1.1 Enlarged nethouse in Southern Italy

1.2 Structural systems

1.2.1 Framed Structures

In general, the agricultural typical structures are classified into three main categories: framed, arched and tensile structures. Framed structures may be found in a single-span or a multi-span form. The widespread structural system consists of moment resisting frames in one direction and braced frames in the other. The shape of the roof may be flat, duopitch or semi-circular and seldom gothic. In addition, the beam elements have hollow galvanized steel sections with thickness larger than 2,0 mm and the usual diameter of columns (CHS) ranges from 50 mm to 120 mm. The connections between steel structural components should be bolted. Welding is an inappropriate solution as it not compatible with the galvanized surface and does not allow the disassembly of the structure.

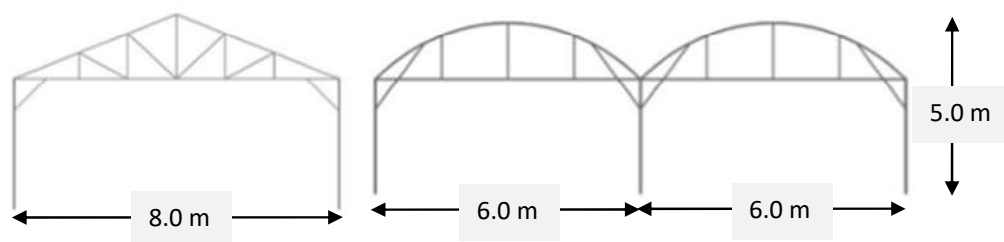


Figure 1.2 Duopitch and arched roofs reinforced with trusses.



Figure 1.3 Nethouse in the form of repetitive Gothic roofs.

1.2.2 Arched Structures

The arched nethouse structures are constructed only in a single-span form with repetitive arches along the longitudinal direction. The feature of arched structures is the development of mainly axial compressive forces, reducing the bending moments under the vertical loads. The stability out of plane, is ensured with braces that are placed in the first and last arch and with beams near to the higher point along the structure. Also, the arched are implemented with steel hollow cross-sections and are curved through an industrial process.

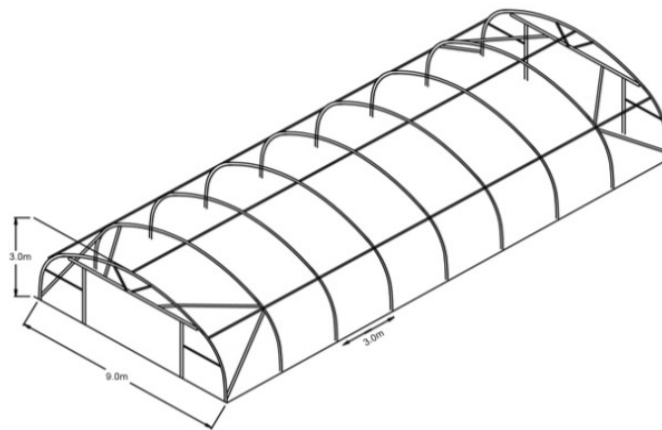


Figure 1.4 Arched (tunnel) nethouse

1.2.3 Tensile Structures

Tensile nethouses are formed with hanging systems in one or two directions consisting of pretensioned steel cables. The main horizontal cables are suspended from steel columns with hollow cross-section and are supported by slope restraining cables anchored to the ground as shown in Figure 1.5. The roof may be flat or duopitch. The inclination of the roof ranges from 15° to 30° and the height of the tensile nethouse is about 5,0m . In many cases, the pretension is imposed in the restraining cables through the lower point and the prestress is applied in the suspension cables indirectly. The prestress contributes to the stability of the columns and the limitation of vertical deformation in the suspension cables. The connection between cables-column is shown in Figure 1.6.

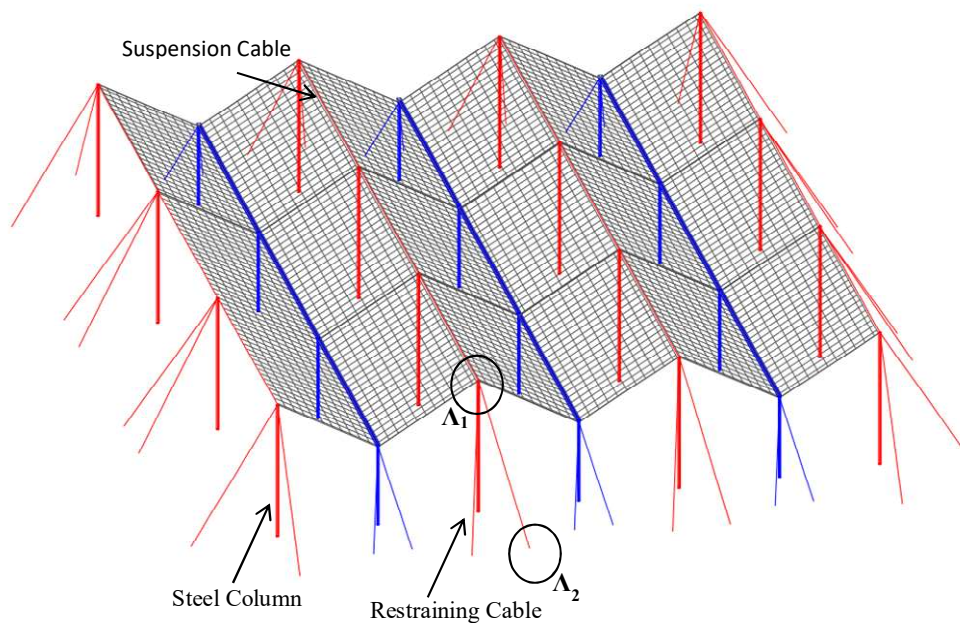


Figure 1.5 Tensile structure for nethouse system

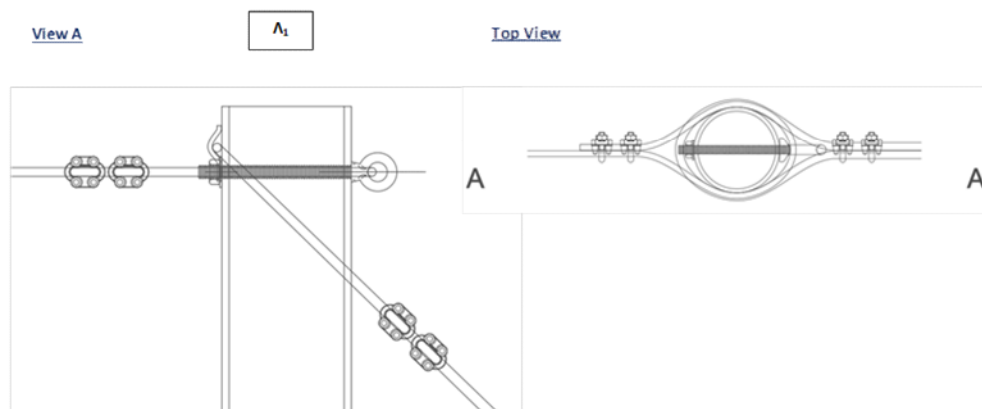


Figure 1.6 Connection between column and cables (suspension, restraining)

In many cases, the pre-tensioning of the cables is applied through special components such as the steel turnbuckles. A turnbuckle is a common rigging device that is used to adjust tension and reduce slack in a rope, cable, or similar tensioning assembly. It is also known as tensioner, barrel strainer or adjuster. Rigging turnbuckles are available in many different types, sizes, but basically there are three primary turnbuckle accessories: a turnbuckle body, a right-hand threaded end fitting, and a left-hand threaded end fitting. Therefore, there are two

main types of turnbuckle body, closed or open. By twisting the turnbuckle body, it can extend or contract the length, without rotating the end fittings, on both sides. The one end is attached to the restraining cable and the other one to anchored body. Essentially, the turnbuckle is an extension of the cable and remains on the construction throughout its life.

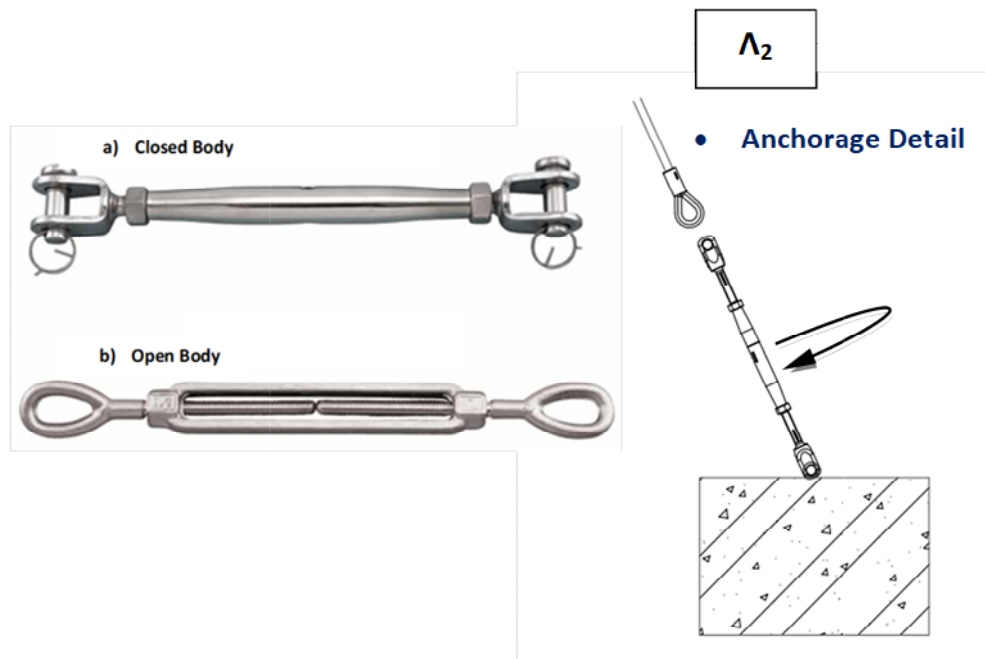


Figure 1.7 The position of the turnbuckle with closed or open body

1.3 Comparison of the structural systems

The choice of the optimal structural nethouse system is associated with the safe leading of the loads (wind, snow, hail, crop load) to the ground with the most economical way obeying agricultural requirements. The tensile structures are the most economical solution because full exploitation of the cross-section occurs as they develop only axial forces (figure 1.8) and have the most competitive material weight-structural capacity ratio. Thus, it is possible to achieve large spans without bending or buckling restrictions. Furthermore, the connections are simple and it is easy to uninstall and erect the nethouse at a new site. In the other hand, the design and the construction requires advanced computational and technical skills as non-linear behavior governs the cables and the prestress makes the erection much more complicated. Undoubtedly, the use of suspension cables constitutes a competitive solution as long as the inevitable large deformations are tolerated.

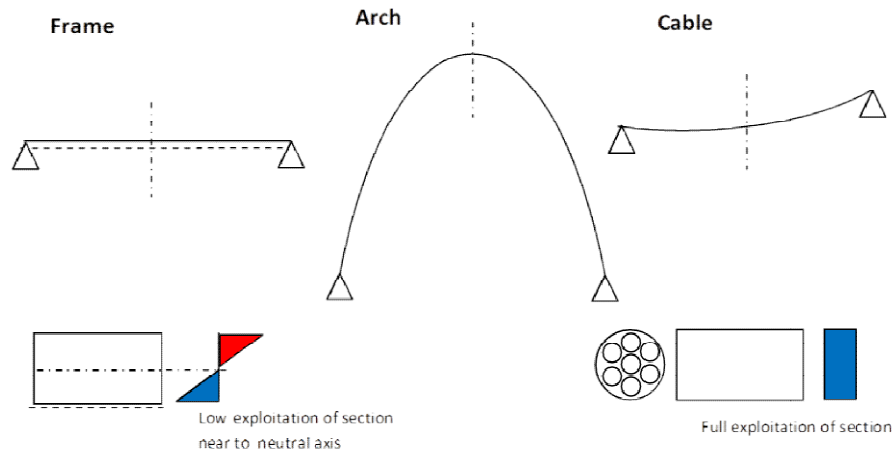


Figure 1.8 Comparison of structural systems

The tunnel (one span) structures are cheaper than the framed ones, because their shape does not allow the accumulation of precipitation (snow, hail) on the roof and also is more aerodynamic which lead to lower structural demands. In terms of functionality, due to the non-uniform height of the arched structure, it is not easy to utilize all the covered land near the curved sides. As well, framed structures are the highest load-capacity system and is the appropriate solution in areas which significant snowfalls occur. But, they are the most complex and heaviest structure system.

2 Materials

2.1 Net

Agricultural nets are extensively used in certain types of structures as cladding material protecting cultivations. It is considered that the net participates in the structural system and it is necessary to examine its static behavior. The transfer mechanism of loads is the biaxial tension and should be modeled as an equivalent orthotropic membrane, a behavior which is mainly due to the way of weaving and production. Structural membranes or nets are characterized by the mesh and the size of their fibers. In Figure 2.1, is presented two commercial agricultural nets under a microscope.

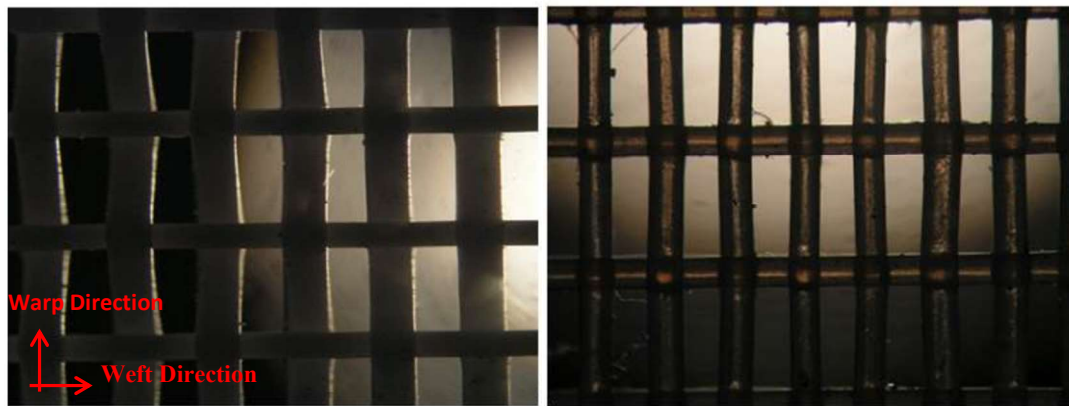


Figure 2.1. Nets Mesh Image under a microscope : a) Ginegar Optinet 50, b) Artes Polytecnica net 50

It is observed that the size and/or mesh density of the fibers is different in the two perpendicular directions. The warp (stiffer) direction coincides with the direction in which the membrane exits the production machine while the other weft (weak) direction is perpendicular to it. In many applications, the material used for the production of agricultural nets is the High Density Polyethylene (HDPE) in a woven or knitted way.

The orthotropic properties of the equivalent orthotropic membranes are expressed in the following plane-stress format :

$$\begin{Bmatrix} \sigma_x \\ \sigma_y \\ \tau_{xy} \end{Bmatrix} = \frac{1}{(1-\nu^2)} \begin{bmatrix} E_x & \nu\sqrt{E_x E_y} & 0 \\ \nu\sqrt{E_x E_y} & E_y & 0 \\ 0 & 0 & \frac{(1-\nu)}{2}\sqrt{E_x E_y} \end{bmatrix} \begin{Bmatrix} \varepsilon_x \\ \varepsilon_y \\ \gamma_{xy} \end{Bmatrix} \quad (2.1)$$

Where E_x , E_y are the modules of elasticity in the two directions and ν is the Poisson's Ratio. In most applications it may be considered as zero value for the Poisson ratio. However, the safest practical method is to perform analyzes with two extreme values of the Poisson's ratio, $\nu=0$ and $\nu=0,4$ and to investigate the most unfavorable situation both in terms of stresses and deformations. As regards the type of the structural analysis, the assumption of a linear elastic material behavior is inaccurate and should be applied a geometrical non-linear analysis (GNA). In Table 2.1, is presented the mechanical properties of the Net (Ginegar Optinet 50) that is used in the analyzes of the present study.

Table 2.1. Mechanical Properties of the Membrane

Ginegar Optinet 50	Elastic Modulus[MPa]	Tensile Strength[MPa]
Longitudinal - Warp	75	25.0
Transverse - Weft	50	15.0

2.2 Cables

The cables have only the tensile stresses as transfer mechanism of loads .Their characteristics are due to the type of their production method, which provide them with significant tensile stiffness but not shear and bending stiffness or resistance to buckling. Due to this weakness, they are forced to adapt their shape to the way external loads are imposed.

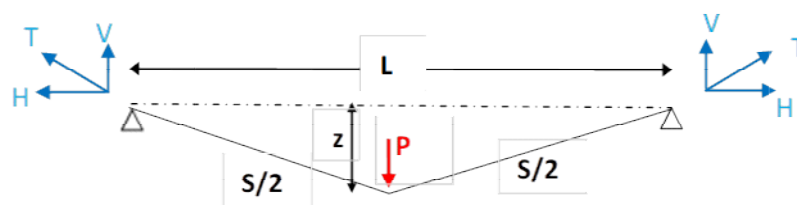


Figure 2.2. The cable under a concentrated load P acting at mid-span

According to the equilibrium (Figure 2.2), the material's constitutive law and the deformation compatibility, which are the three sources of equations in the non-linear structural analysis, the equation path is :

$$P = 2EA \left(\frac{z}{S_0} - \frac{1}{\sqrt{z^2 + \frac{L^2}{4}}} \right) z \quad (2.2)$$

where EA is the axial stiffness of the steel cross section, S_0 is the initial undeformed length of the cable and L is the length of the span. In Figure 2.3 is presented the graph of equation (2.2) and shows that the cable response is not linear. It is observed that the cable response becomes stiffer as the load and corresponding deflection increase. This can be explained by the observation that the vertical component of the inclined cable's internal force on both sides increases and the external load is more directly balanced (Figure 2.2).

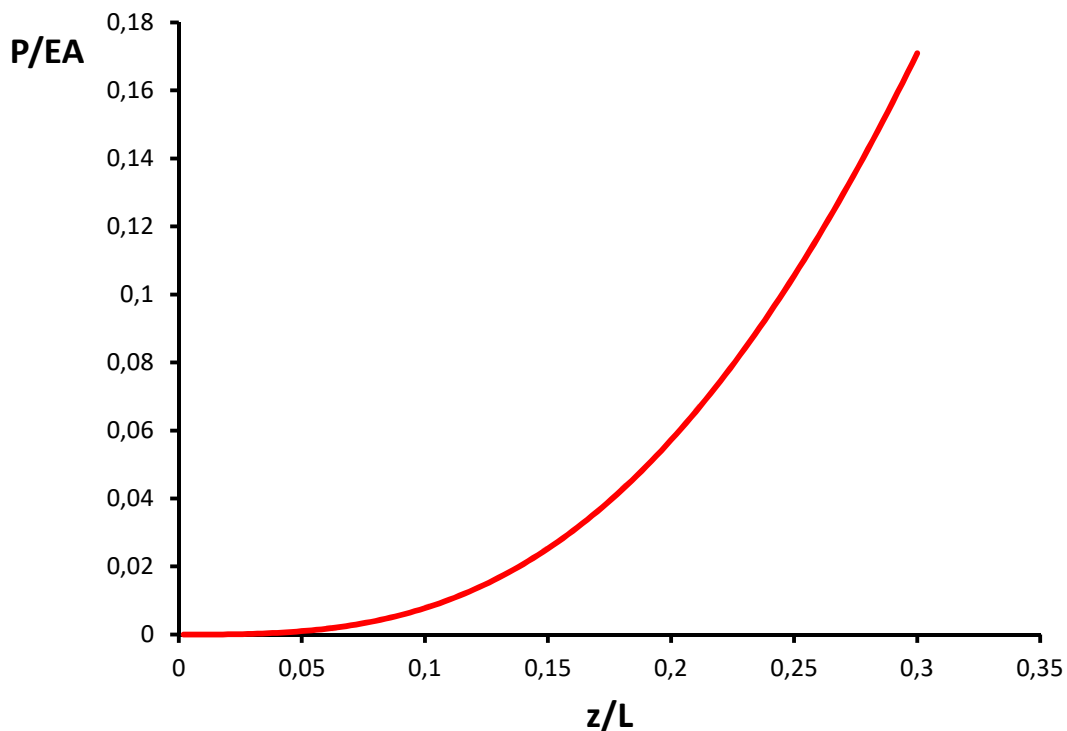


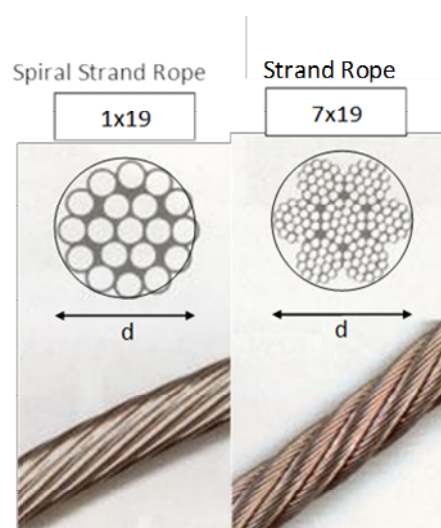
Figure 2.3. Equation Path of the cable

The European Standard EN 1993-1-11, gives design rules for structures with prefabricated tension components made of steel. In the Table 2.2, are mentioned all the different types of cables.

Table 2.2 Group of tension Components

Group	Main tension element	Component
A	rod (bar)	tension rod (bar) system, prestressing bar
B	circular wire	spiral strand rope
	circular and Z-wires	fully locked coil rope
	circular wire and stranded wire	strand rope
C	circular wire	parallel wire strand (PWS)
	circular wire	bundle of parallel wires
	seven wire (prestressing) strand	bundle of parallel strands

In this study, the cables in group B were used. In particular, those cables that are formatted as spiral strand ropes. Strand is an element of rope normally consisting of an assembly of wires of appropriate shape and dimensions laid helically in the same or opposite direction in one or more layers around a center. In most cases, each strand consists of 19 or 37 wires. The Spiral Strand Rope is an assembly of one strand, while the Strand Rope consists of several strands (7) laid helically in one or more layers around a core (center strand).

**Figure 2.4.** Usual types of cables, Group B

In addition, it should be emphasized that the cross-section of the tensile component of group B is not completely full and is given as follows:

$$A_m = \pi \frac{d^2}{4} f \quad (2.3)$$

where d is the external diameter, including any sheathing for corrosion protection and f is the fill factor.

Table 2.3 The fill factor of cross section for Group B

TYPE	FILL FACTOR f			
	Number of wire layers around core wire			
	1	2	3-6	>6
Spiral Strand Rope	0,77	0,76	0,75	0,73

Regarding the modulus of elasticity for Group B tension components should be derived from test. It depends on the stress level and whether the cable has been prestretched and cyclically loaded and unloaded. When test results are not available, nominal values of moduli of elasticity for use as first estimates are given in EN 1993-1-11, (Table 3.1). For Spiral Strand Rope with steel wires:

$$E = 150GPa \quad (2.4)$$

In context of the present dissertation, it was used cables with yield limit $f_y=1520MPa$ and full elastic behavior. In figure 2.5 is presented the corresponding Material Constitutive Law.

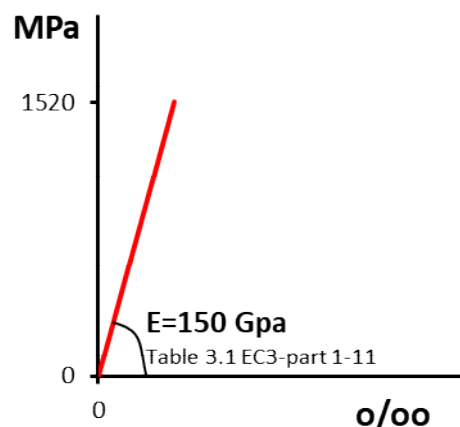


Figure 2.5 Material Law of the cable

3 Structural analysis

3.1 Methodology

In order to predict the actual collapse load of the slender steel nethouse support systems, a nonlinear analysis should be performed. The prediction of collapse, especially when cables are involved in the static system, is a highly nonlinear phenomenon and the elastic linear analysis is inappropriate. Collapse may occur due to exceeding the developed stresses beyond the material capacity at certain cross section, a condition known as material nonlinearity, or due to buckling, associated with a steep increase in deformation for a small increase in imposed load, a condition known as geometric nonlinearity.

The first step is to perform linearized buckling analyses (LBA) through that the critical buckling modes and corresponding loads are determined. In most cases, the critical buckling loads are not a safe prediction of the structure strength and consist of an initial indication as an upper bound of the actual strength. In addition, the buckling modes (shape of deformation) are useful tools of understanding the way of the collapse.

To identify the crucial failure mechanism, a nonlinear analysis should be performed, including the large displacement effect (geometric nonlinearity) and the material behavior beyond the elastic range (material nonlinearity). The aforementioned nonlinear analysis is called (GMNA). Furthermore, the real structures have initial imperfections deviating from the perfect geometry and should be taken into account in the calculation of the strength. The shape of the imperfections may be chosen according to the buckling modes (LBA). Hence, a geometrical and material nonlinear imperfection analysis (GMNIA) is recommended for reliably evaluating the strength and safely avoiding the instability effects of steel structures.

In the contexts of this thesis, the numerical algorithm extensively used for nonlinear structural analysis is the full-Newton-Raphson. The quadratic convergence rate of the Newton method guarantees convergence within few iterations and is the main reason for its universal implementation in almost all commercial FEA software. In Newton's method, the load increases incrementally. The external load vector \mathbf{F}^{ext} is gradually increased in order to reach a desired value \mathbf{F}^{d} . Introducing a scalar quantity λ can control the load incrementation and the potential equilibrium equation of the system is:

$$\mathbf{R}(\mathbf{u}) = \mathbf{F}^{int}(\mathbf{u}) - \mathbf{F}^{ext} \Rightarrow$$

$$\mathbf{R}(\mathbf{u}) = \mathbf{F}^{int}(\mathbf{u}) - \lambda \mathbf{F}^{ext} = \mathbf{0} \quad (3.1)$$

In the general case, the system of equations is not in equilibrium and the difference $\mathbf{R}(\mathbf{u})$, expresses the residual vector, which is then used to find corrections in the solution. At each increment, the value of λ changes and the algorithm tries to determine the corresponding \mathbf{u} so that the system in (3.1) is satisfied. Assuming that the last converged solution is $\{\mathbf{u}_0, \lambda_0\}$, the load incrementation occurs as follows :

$$\lambda' = \lambda_0 + \Delta\lambda \quad (3.2)$$

where $\Delta\lambda$ is a known predefined incrementation parameter. So, it is necessary to update the displacements \mathbf{u}_0 by :

$$\mathbf{u}' = \mathbf{u}_0 + \Delta\mathbf{u} \quad (3.3)$$

so that,

$$\mathbf{R}(\mathbf{u}') = \mathbf{R}(\mathbf{u}_0 + \Delta\mathbf{u}) = 0 \Rightarrow \mathbf{F}^{int}(\mathbf{u}_0 + \Delta\mathbf{u}) - (\lambda_0 + \Delta\lambda)\mathbf{q} = \mathbf{0} \quad (3.4)$$

But, $\mathbf{F}^{int}(\mathbf{u}_0 + \Delta\mathbf{u})$ can be expressed in terms of $\mathbf{F}^{int}(\mathbf{u}_0)$ by a Taylor series expansion as :

$$\mathbf{F}^{int}(\mathbf{u}_0 + \Delta\mathbf{u}) = \mathbf{F}^{int}(\mathbf{u}_0) + \left[\frac{\partial \mathbf{F}(\mathbf{u})}{\partial \mathbf{u}} \right]_{\mathbf{u}_0} \Delta\mathbf{u} = \mathbf{F}^{int}(\mathbf{u}_0) + [\mathbf{K}_T]_{\mathbf{u}_0} \Delta\mathbf{u} \quad (3.5)$$

where $[\mathbf{K}_T] = \left[\frac{\partial \mathbf{F}(\mathbf{u})}{\partial \mathbf{u}} \right]$ is the ‘Jacobian’ matrix of system of equation and is referred to as the Stiffness Matrix. Combining equation (3.4) and (3.5), we can solve for $\Delta\mathbf{u}$ as:

$$\mathbf{F}^{int}(\mathbf{u}_0) + [\mathbf{K}_T]_{\mathbf{u}_0} \Delta\mathbf{u} - (\lambda_0 + \Delta\lambda)\mathbf{q} = \mathbf{0} \Rightarrow \mathbf{F}^{int}(\mathbf{u}_0) - \lambda_0 \mathbf{q} + [\mathbf{K}_T]_{\mathbf{u}_0} \Delta\mathbf{u} - \Delta\lambda \mathbf{q} = \mathbf{0} \Rightarrow$$

$$\Delta\mathbf{u} = [\mathbf{K}_T]_{\mathbf{u}_0}^{-1} (\Delta\lambda \mathbf{q}) \quad (3.6)$$

From equation (3.6), it is calculated the displacement correction $\Delta\mathbf{u}$. Evaluating the equilibrium at the new point (\mathbf{u}', λ') a non-zero residual vector $\mathbf{R}(\mathbf{u}')$ is obtained. Using this residual vector, we can calculate a new displacement correction $\delta\mathbf{u}$ as follows :

$$\mathbf{R}(\mathbf{u}_0 + \Delta\mathbf{u} + \delta\mathbf{u}) = \mathbf{0} \Rightarrow \mathbf{F}^{int}(\mathbf{u}_0 + \Delta\mathbf{u}) + [\mathbf{K}_T]_{\mathbf{u}'} \delta\mathbf{u} - (\lambda + \Delta\lambda)\mathbf{q} = \mathbf{0} \Rightarrow$$

$$[\mathbf{K}_T]_{\mathbf{u}'} \delta\mathbf{u} = -[\mathbf{F}^{int}(\mathbf{u}_0 + \Delta\mathbf{u}) - (\lambda + \Delta\lambda)\mathbf{q}] \Rightarrow [\mathbf{K}_T]_{\mathbf{u}'} \delta\mathbf{u} = \mathbf{R}(\mathbf{u}') \Rightarrow$$

$$\delta\mathbf{u} = [\mathbf{K}_T]_{\mathbf{u}'}^{-1} \mathbf{R}(\mathbf{u}') \quad (3.7)$$

Thus, a new displacement correction is obtained and evaluating the system (3.4) at new point $(\mathbf{u}' + \delta\mathbf{u}, \lambda')$ that lead to a new smaller residual vector $\mathbf{R}(\mathbf{u}'')$. This process continues until a norm of the residual vector is less than the specified tolerance. A descriptive representation of the Newton-Raphson method is shown below.

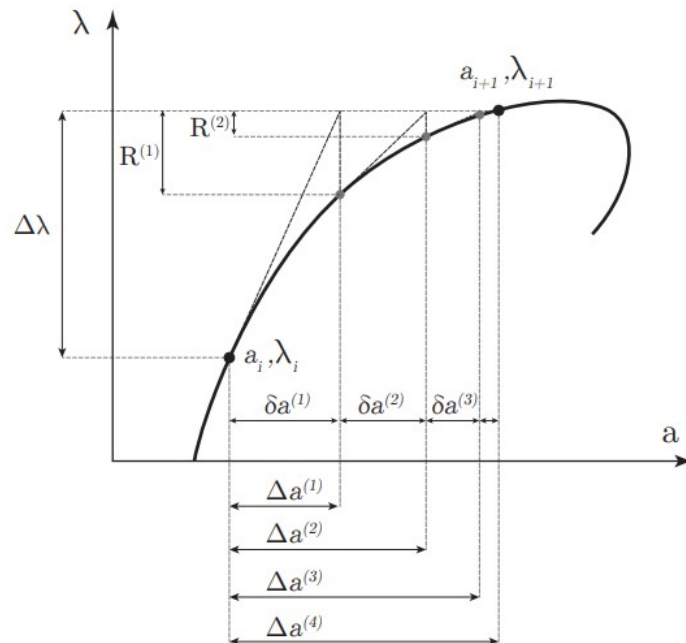


Figure 3.1 The representation of the Newton-Raphson method

3.2 Structural Model

The investigation of static behavior of nethouses will take place through an enlarged parametric and comparative analysis that will signalize the most critical parameters of the structural design. For this reason, a simple finite element model is created that consists of the main substructure of the nethouse (columns, cables). The analysis should take into account the transient construction phase including the sequential placement of the members, the pre-tensioning of the cables and the final form finding of the geometric structure. In particular, the order of the construction stages is the installation of : the steel columns at distances, the suspension cable, and lastly the inclined restraining cables, two on each side. The prestress is inserted into the system through the lowest point of each restraining cable. Therefore, the suspension cable is indirectly prestressed. Figure 3.2, shows the sequence of construction phases.

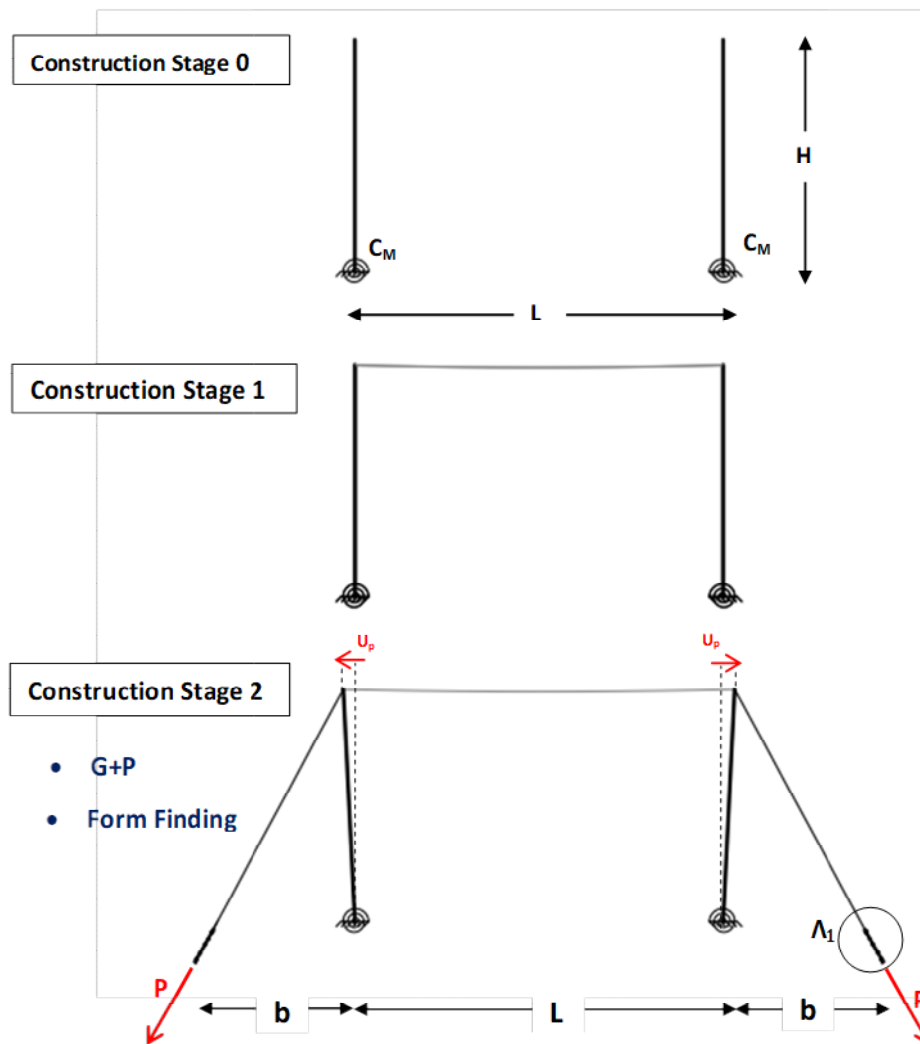


Figure 3.2 The sequence of the construction stages

After form finding is completed, the structural model is subjected to service loads and a static analysis is performed, starting from the configuration under the gravity loads "G" and prestressing "P" that should be combined in a single permanent action. It is emphasized that only vertical loads (in plane) are considered and the expected deformation shape under increasing loads, is shown at the bottom of Figure 3.3.

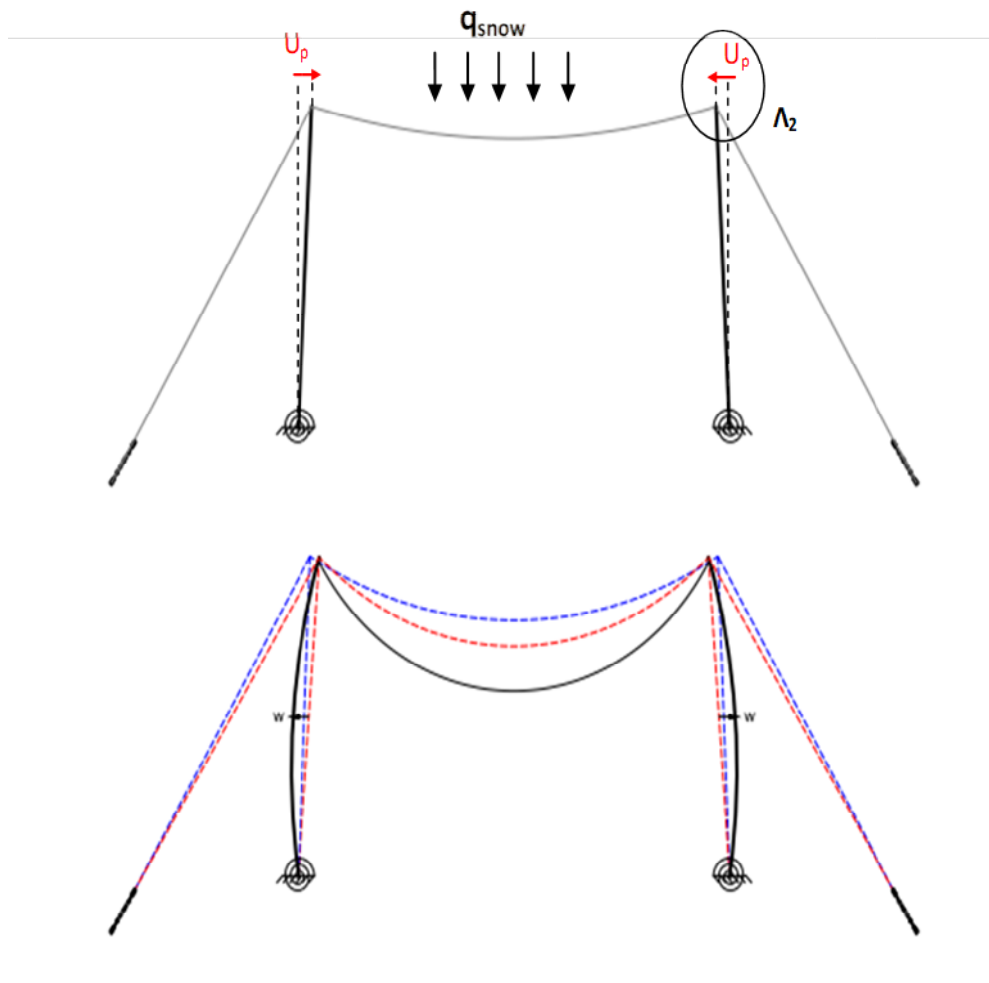


Figure 3.3 Deformed shape of structural model under snow loads

The columns are modeled as beam elements while the wire ropes as cable elements. The cross sections of the structural components are mentioned in the table 4.

Table 3.1 Cross sections

Cross-Sections	
Column CHS	D=88.9x4.0 mm (class I)
Restraining Cable	D ₁ =20 mm
Suspension Cable	D ₂ =10 mm

It is considered that the structural response is fully characterized by both the vertical displacement in the middle of the cable and the rotation of the column head. For this reason,

the equilibrium paths are recorded at the aforementioned degrees of freedom indicating the failure mechanisms of the system. During the parametric analysis, the main variables are the angle θ , the magnitude of the prestressing as well as the boundary conditions of the column. As standard dimensions, the height of columns (5 m) and the length of the span (8 m) remain constant. The finite element model is set up in the German Software Sofistik and it is detailed below.

Model

- Record ϕ , U_z

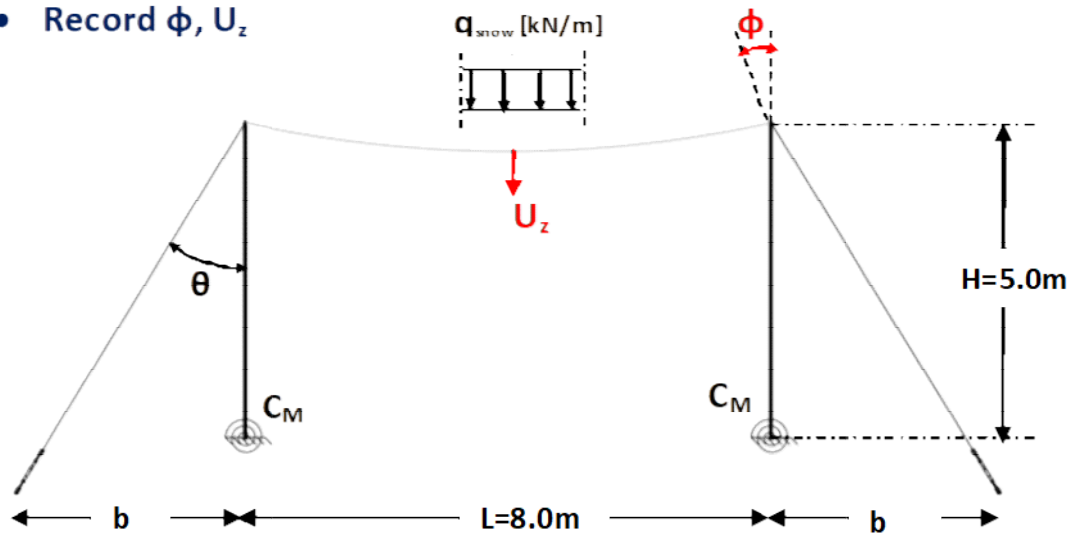


Figure 3.4 Finite element model

3.3 Investigation of nonlinearity

According to the methodology developed in subchapter 3.1, a linearized buckling analysis is performed (LBA). For simple cases of individual columns, the critical buckling load coincides with the Euler load. For a simply supported beam-column, the Euler load is:

$$P_{cr} = \pi^2 EI / L^2 \quad (3.8)$$

and in the examined case, with CHS 88.9x4.0 as cross section of the column:

$$P_{cr} = \frac{\pi^2 (2.02 \cdot 10^2)}{5^2} = 79.87 kN$$

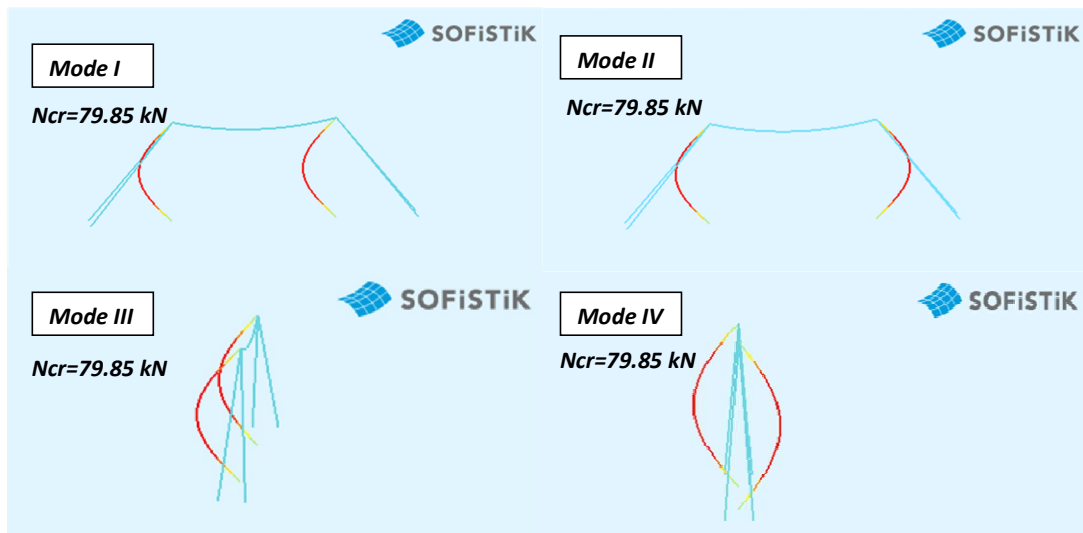


Figure 3.5 The critical buckling modes and corresponding loads by means of LBA

In case of pinned columns integrated in the static system, it is observed that the first four buckling modes have as critical load the corresponding Euler load as calculated in equation 3.8. The strength evaluation should always be based on nonlinear analyses, accounting for both types of nonlinearity (GMNA). Nevertheless, it is useful to carry out first separate analyses accounting only for material nonlinearity (MNIA) and/or geometric nonlinearity (GNIA), that help us to understand which one dominates.

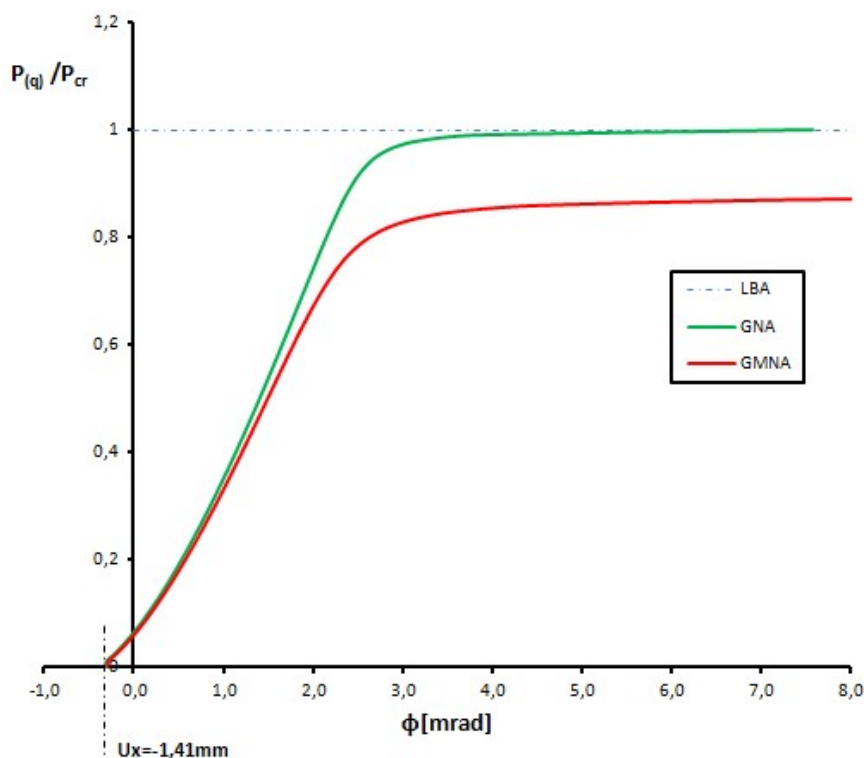


Figure 3.6 The equilibrium paths of the column

In figure 3.6, it is presented the equilibrium paths by means of GNA and GMNIA. It is observed that both nonlinearities affect the response of the system as defined by the red line of the diagram. The response does not start from the beginning of the axes which is due to the prestressing and the initial deviation of the column head from the perfect geometry is $u_x=1.41\text{mm}$. The system parameters, as defined in Figure 3.4, for the above analyzes are listed in Table 3.2.

Table 3.2. The parameters of the structural system

Parameters	
H[m]	5,0
b[m]	4,0
a[m]	0,5
θ [°]	38,6
P[kN]	3,0
C_M [kNm/rad]	1,0
d_1 [mm]	20,0
d_2 [mm]	10,0
D_{column} [mm]	88,9
t_{column} [mm]	4,0

3.4 Influence of the anchor angle θ

An important design parameter is the angle θ of the inclined restraining cables formed within the load plane. By increasing the angle θ , the horizontal component of the axial force of the inclined restraining cable increases and due to this, the suspension cable becomes more stiff under the vertical loads. For exactly the same reason, the vertical component of the inclined cable is reduced and the column is relieved by additional compressive axial force. Hence, increasing the angle θ is beneficial for the static behavior of the system for both the suspension cable and the column. In the present analyzes, it is noted that the column is simply supported and its bending and shear stiffness are not activated for carrying the loads.

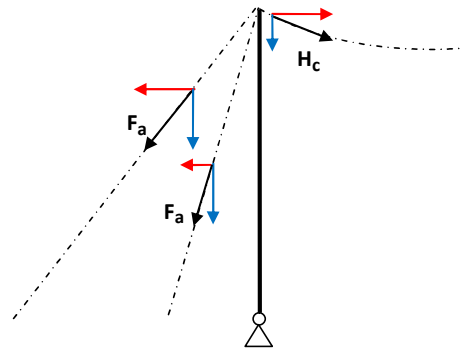


Figure 3.7. The components of the forces of the cables

To quantify the positive influence of the increase of the angle θ , nonlinear analyses were performed for different angles keeping all the other parameters constant. In Figures 3.8,3.9, the equilibrium paths are obtained by means of the geometrical and material nonlinear analyses (GMNA). Curves with the same color correspond to the same analysis but to a different degree of freedom.

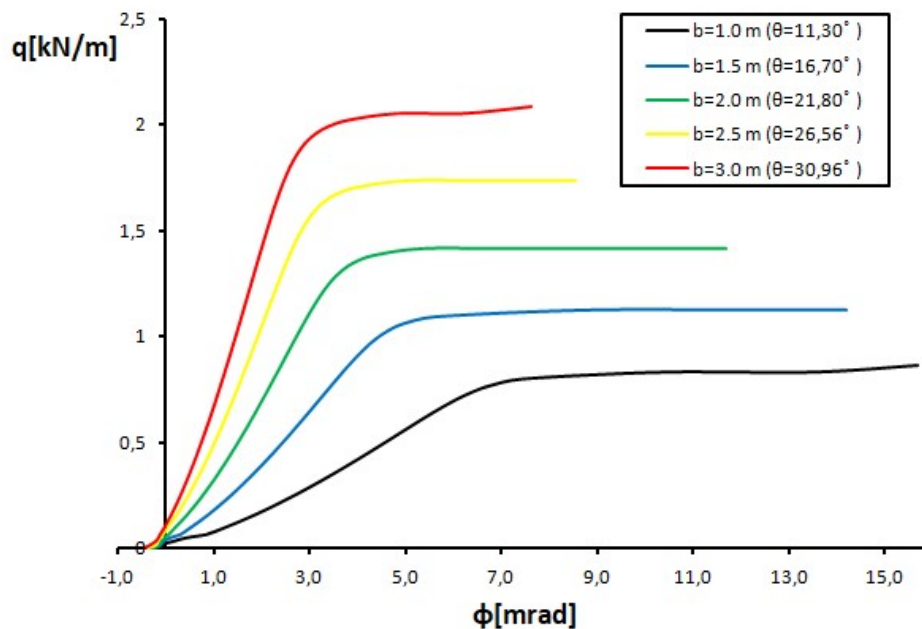


Figure 3.8 The influence of increasing the angle θ on the static behavior of the column

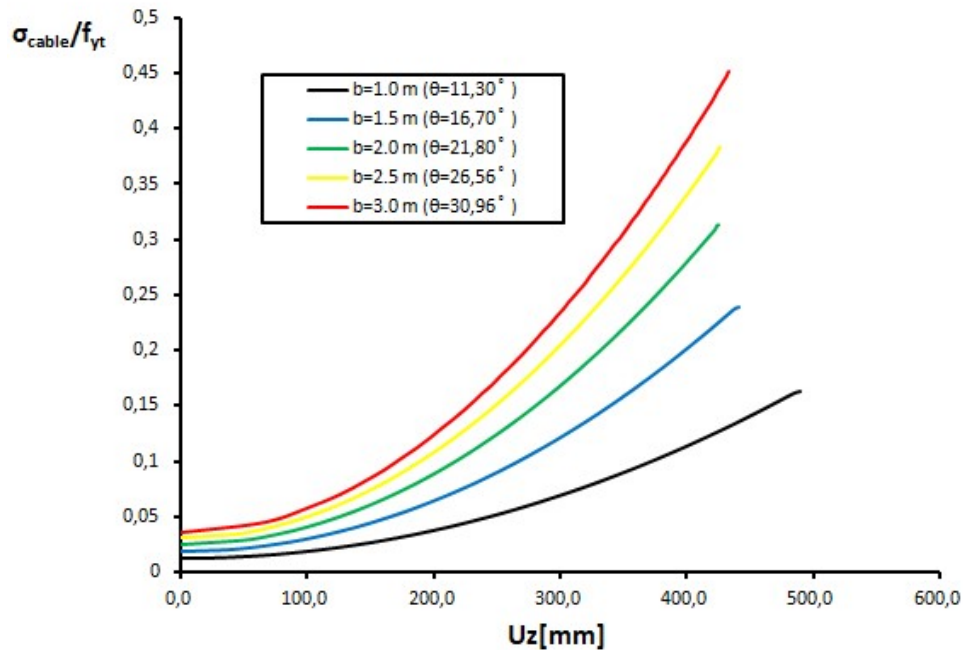


Figure 3.9 The influence of increasing the angle θ on the static behavior of the suspension cable

3.5 Influence of prestressing

The magnitude of the prestressing is a main design parameter and should be adjusted accordingly. It is recommended by the instructions (EN EC3-1.11) that the cables are pre-stretched up to a maximum of 45% of the breaking force. In the present case, the restrictions of the prestressing equipment (turnbuckles) determine the maximum possible force of the prestress cable. Typical prestressing values range from 2 to 20 kN.

By increasing the prestressing force, the vertical deformations of the suspension cable are reduced, however, the column is subjected to increased axial force leading faster to buckling. Hence, the optimal magnitude of the prestressing force should be obtained by an overall evaluation of the data. Observing the diagrams in Figures 3.10 and 3.11, it is concluded that in each case of the magnitude of the pre-tension, the weak member is the column.

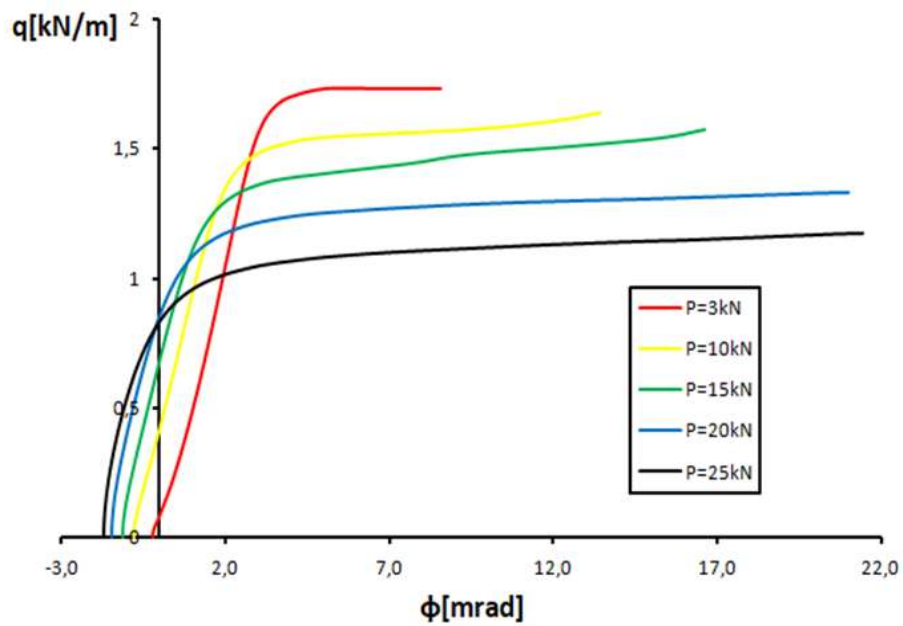


Figure 3.10. The influence of the magnitude of the prestressing force on the static behavior of the column

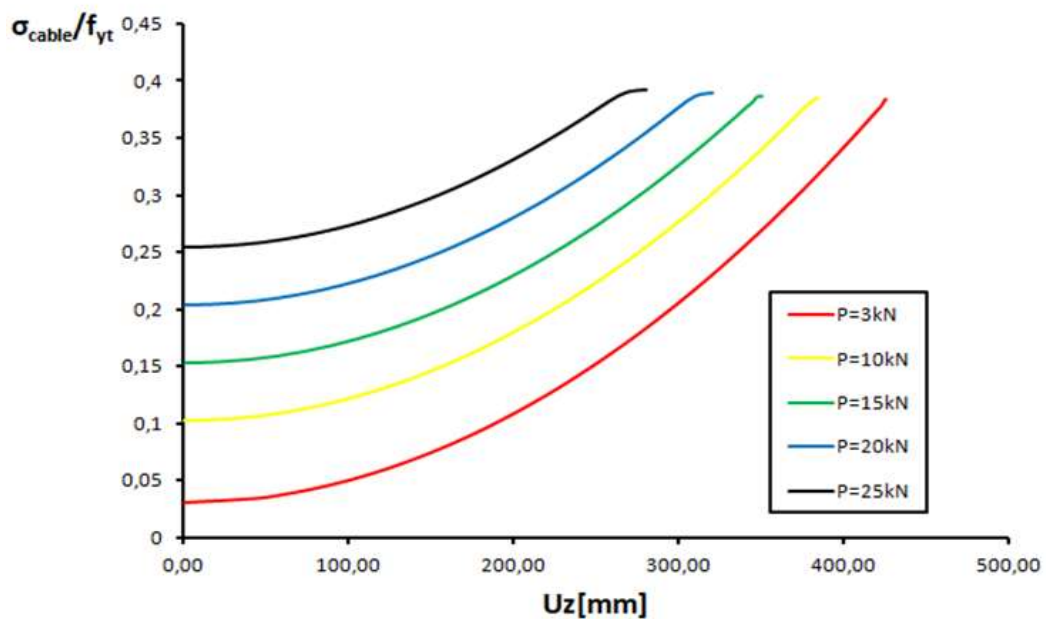


Figure 3.11 The influence of the magnitude of the prestressing force on the static behavior of the suspension cable

3.6 Influence of imperfections

The total evaluation of strength should be obtained by means of a geometrically and material nonlinear imperfection analysis (GMNIA). The assumed shape of the imperfections is accordingly defined by the first buckling mode (fig 3.5,LBA). Figure 3.12 shows the parametric analysis, regarding the influence of size of initial local bow imperfection e_0/L , including the residual stresses and geometrical imperfection effect.

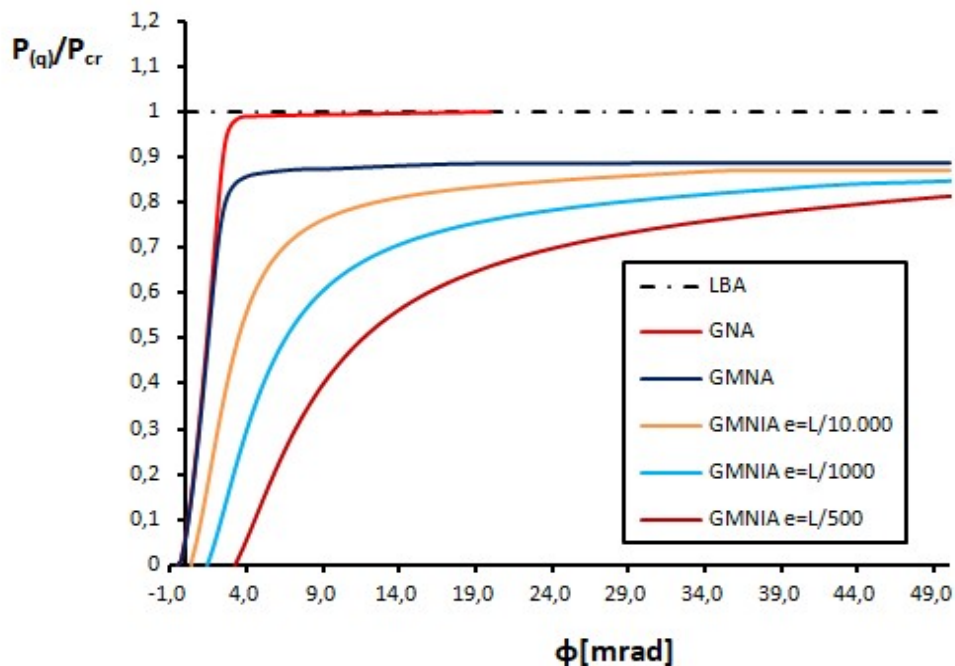


Figure 3.12 Parametric analysis about the size of imperfections

It is observed that the postbuckling equilibrium path is stable and the effect of imperfections is significant, affecting the strength of the structure. Moreover, in an attempt to identify the most unfavorable situation, the direction of the imperfection of columns regarding their relative position should be investigated. In figure 3.13, the corresponding examination is presented.

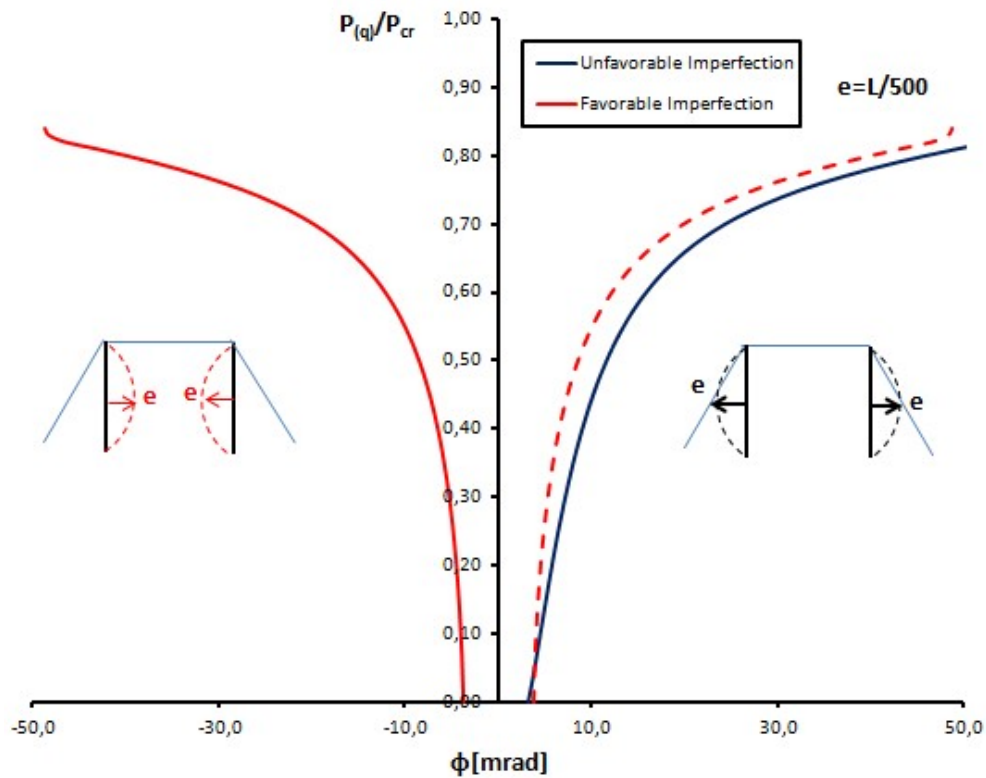


Figure 3.13 Investigation about the direction of the imperfection

In the chart above, the blue line represents the equilibrium path of the outer bow imperfection case and the red line describes the inner one. Comparing the two lines in the same plane, it is concluded that the first case is the most crucial.

3.7 Sub-model of membrane

The agricultural net is a cladding material but participates in the structural system. For this reason, it is essential to investigate its static behaviour and determine the way loads are transferred from net to cables. Therefore, a finite element model is created in Ansys that consists of three duopitch panels. In structural modelling, the cables and the net share the same degrees of freedom, except for the longitudinal displacement u_x (fig 3.12). The inclination angle of the flexible roof is $\varphi=30^\circ$ and each part of it has a dimension of 4mx8m.

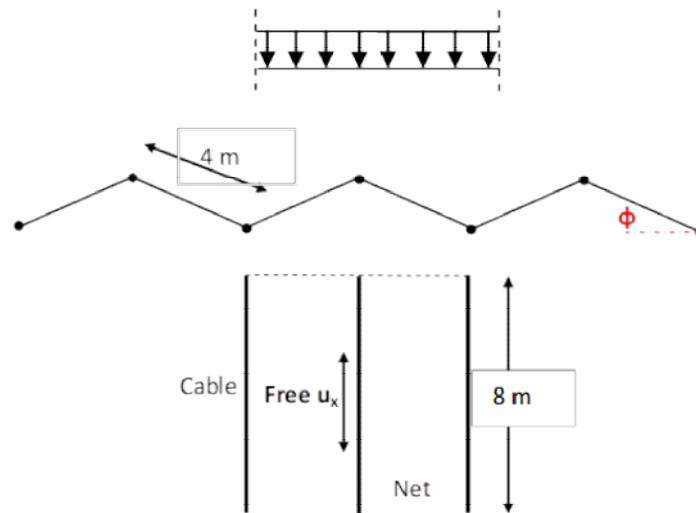


Figure 3.14 Sub-model of membrane

The Von Mises stresses of the one-way nethouse roof under the load level equal to $q=0.5\text{kN/m}^2$ and the corresponding total deformation are displayed in the figure 3.15 and 3.16 respectively. The maximum equivalent stresses are developed on the edges of the cables ($\sigma_{\text{max,von mises}}=11,0 \text{ MPa}$), while the maximum total deformation is observed in the middle of the span.

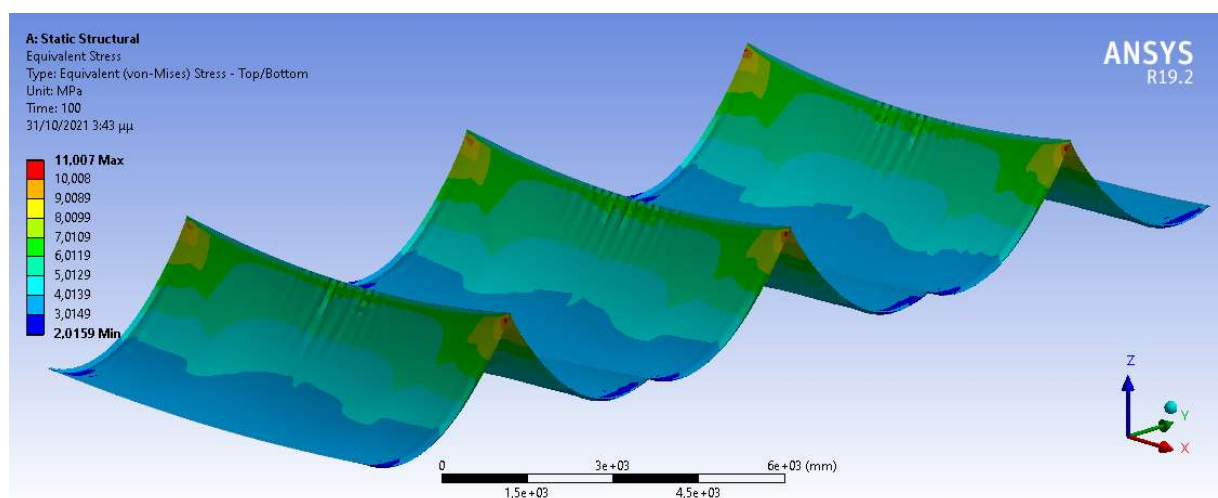


Figure 3.15 Equivalent Von Mises stresses of flexible roof

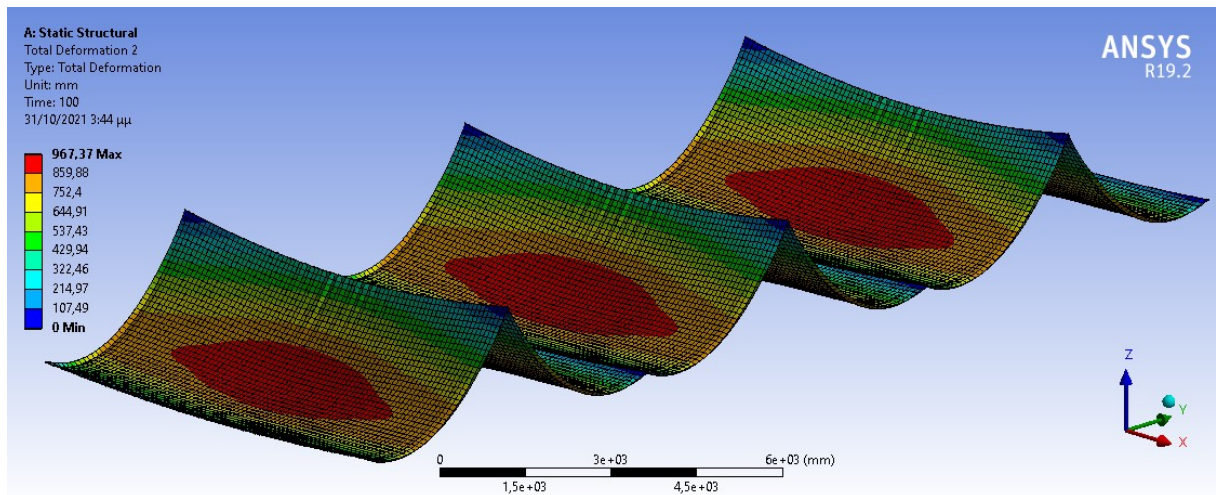


Figure 3.16 Total deformation of flexible roof

The practical load distribution in an one-way roof is assumed to be uniform, as represented by the black line in figure 3.17. Considering cable and net stiffness of the structural model, the real load distribution obtained by Ansys is now represented by the red line in the same chart. The area enclosed by the red line is equal to that below the black line.

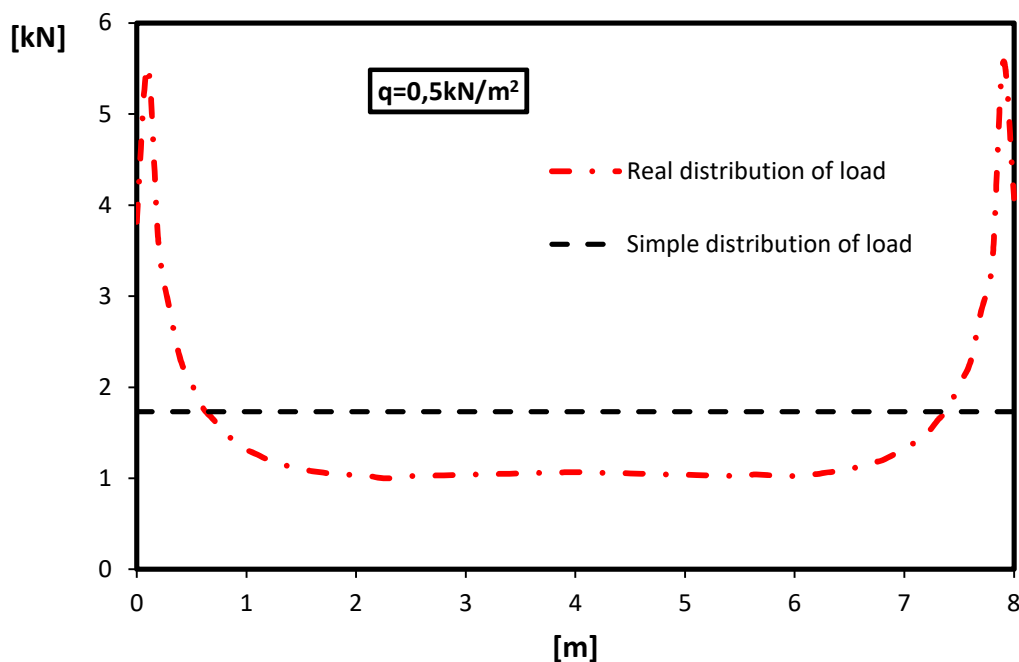


Figure 3.17 Load distributions on flexible roof

Further investigating the way in which loads are transferred from net to cables, analyzes for several load levels are carried out and their distributions are shown in figure 3.18. The load is concentrated at the ends of the cable where it is most stiff.

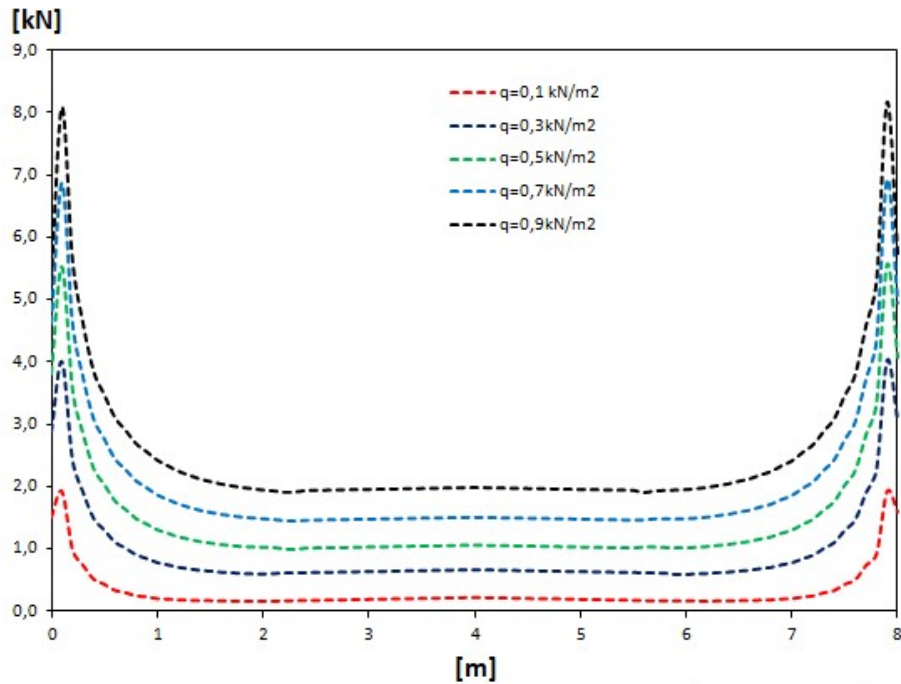


Figure 3.18 Load distributions on flexible roof for several load levels

The net is not constrained along the length of the cable. Actually, net is supported in discrete points per predefined distance, using special grips (fig. 3.19). To identify the influence of this distance, two different cases (0.5m, 1.0m) are examined.



Figure 3.19 Special grips

In the figures below 3.20, 3.21 the equilibrium path for possible distributions of load are shown for the column and cable respectively. It is detected that the case of supporting per 1.0 m distance is the most unfavorable, while the case of the load distribution that is given in figure 3.17 is the most favorable.

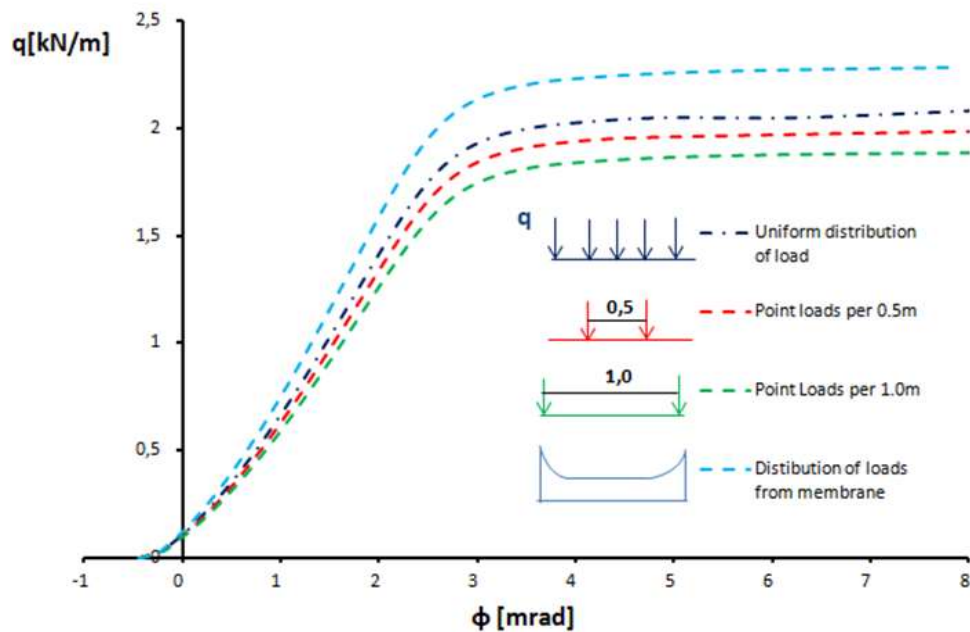


Figure 3.20 Equilibrium path of column for different distribution of load

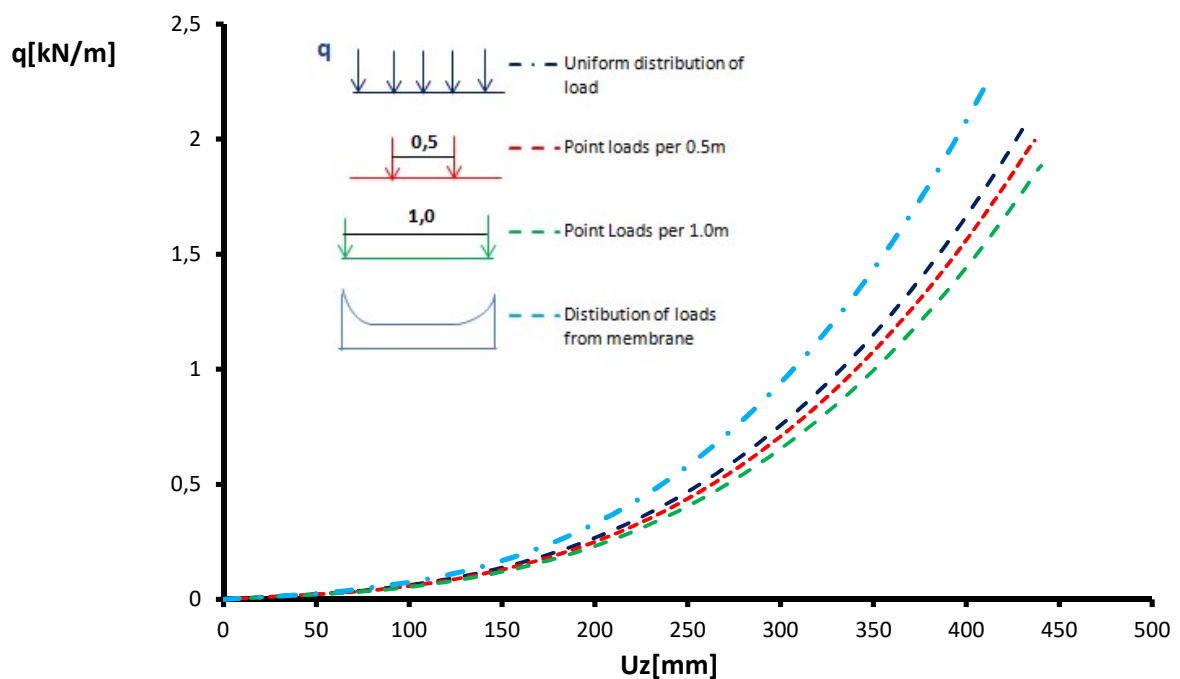


Figure 3.21 Equilibrium path of cable for different distribution of load

3.8 Aggregate results

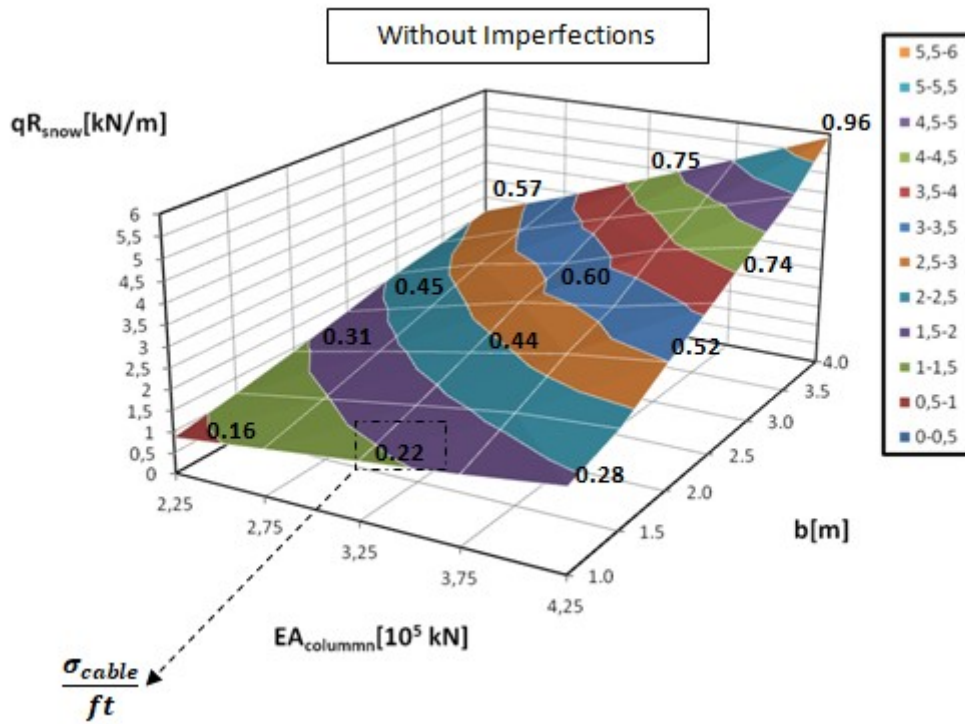


Figure 3.22 Aggregate results without imperfection

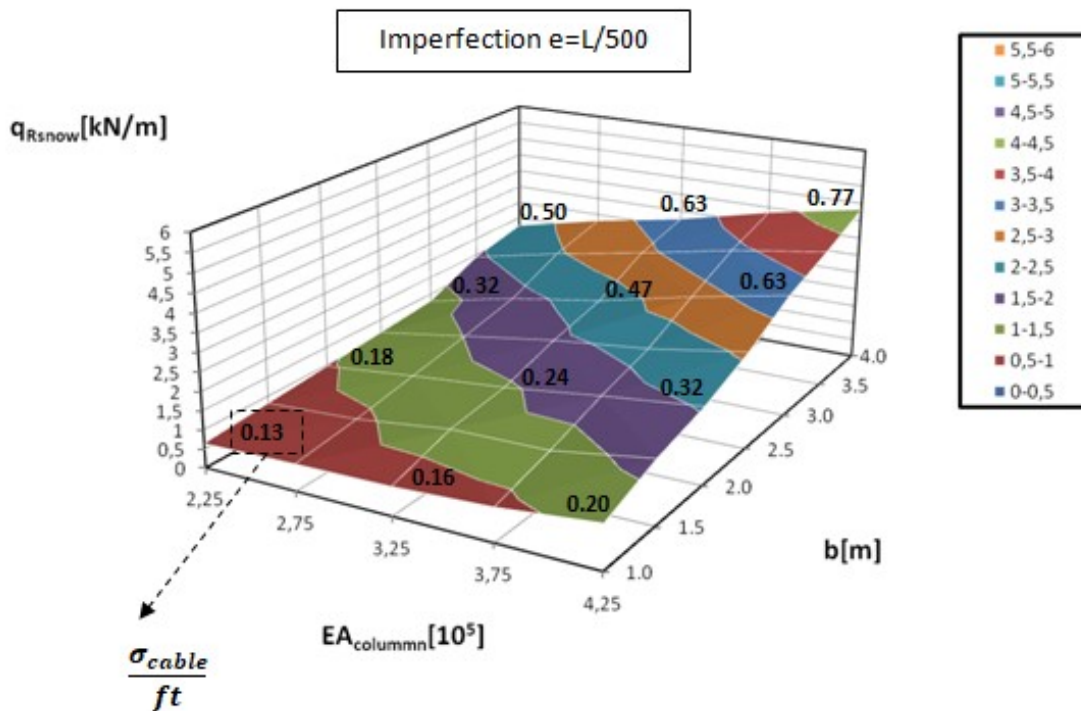


Figure 3.23 Aggregate results with imperfection $e_0=L/500$

4 Description of the release mechanism

4.1 The necessity of the release mechanism

The nethouses are agricultural lightweight steel structures that intent to protect the crops against climatic hazards. Up to now, they are not designed for snow loads and as a result their use is either restricted or unsafe. In many cases though, the probability of snow or hail loads is significant. Thus, it is necessary to take them into consideration for design purposes. For safety purposes, a nethouse under such loads without being supported by an expensive structural system should be designed with an innovative overload release mechanism. This release mechanism should be able to open, forbid any potential overload and thus, to relieve the structural system. The desired outcome of the innovative design of the release mechanism is the structural independency of the mechanism, which will ensure that the bearing members of the main structure (cables, columns, etc.) will not have to be modified in order to include the release mechanism or to carry the extra snow/hail loads. Such a design would render the release mechanism applicable for the entire Greek territory, irrespective of the local climatic conditions.

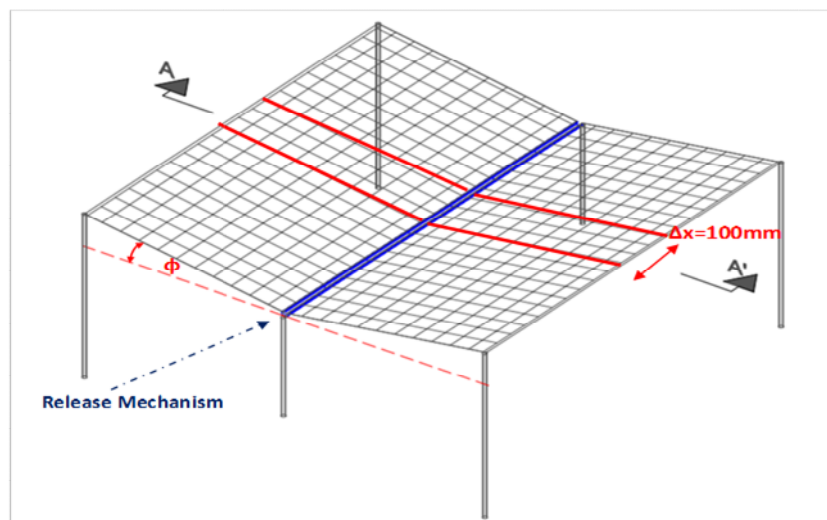


Figure 4.1. The position of the release mechanism along of the duopitch structure.

Initial investigations on the structural supporting system have shown that a duopitch nethouse is the preferable geometrical configuration for nethouses in Greece. The release mechanism should be located near the lowest point of the duopitch roof (gutter), where hail or snow accumulation occurs.

4.2 Requirements of the release mechanism

The release mechanism should be composed of distinct components while its operation should be as simple as possible. The incorporated mechanism must be able to deform as the load increases and release the accumulated load automatically, without human intervention, when the load exceeds a predefined limit-value. It is worth mentioning that during a heavy snowfall, the mechanism may not be possible to manually open. An important design aspect is that after the release, the mechanism should be easily reassembled without any kind of structural damage or modification. In addition, a crucial design requirement is that the anti-insect protection should not be affected by the presence of the release mechanism. This can be avoided through a mechanism that offers overlapping of the neighboring net-segments along the structure. The existing typical release (anti-hail) mechanisms work properly, however they do not meet two basic criteria mandatory for nethouses. The first criterion is that the release mechanism should not interfere with the nethouse's insect-proof ability (presence of open gaps between the mechanisms, Figure 4. left) before its full release and the second one is that its operation should be automatic and not manual. Typical examples missing the aforementioned criteria are shown in Figure 4..



Figure 4.2 Release mechanism with low anti-insect protection (left); manual removal (right)

4.3 Specifications

The configuration of the proposed mechanism consists of a semicircular clip which is applied to a flexible pipe. The structural pretensioned cable passes through the hollow section of the pipe. The pipe is supposed to be relatively flexible and it is considered as a non-structural element. The clip and the pipe have similar diameter. The agricultural insect-proof

nets are placed between the clip and the pipe and so the entire system (clip, net, pipe) becomes stable (Figure 4.). The clip is continuous along the length of the pipe maintaining the anti-insect character of nethouses. The proposed mechanism could be implemented in different roof slopes.

The components of the proposed release mechanism are made of polyvinyl chloride (PVC) or polypropylene (PP). Both materials are widely produced and used in variety of applications. Either of the two materials would be a low cost and practical solution for the design of the release mechanisms. From the structural point of view, the mechanism should work elastically, so that the structural demands will be precisely defined, independent from safety factors, overstrength, etc. Hence, the most important material property for the functionality of the release mechanism is the Young's modulus E (GPa). For PVC and PP materials the Young's Modulus ranges between the values $E=1 - 4$ Gpa. The components of the mechanism and the geometrical configuration are described in Figure 4..

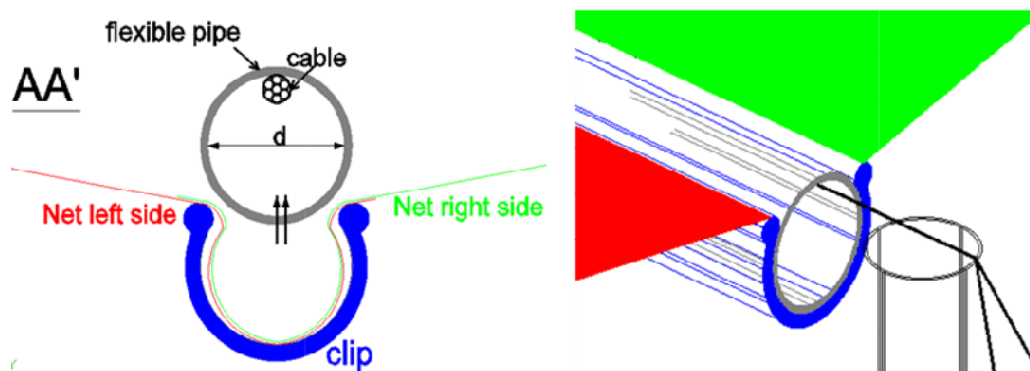


Figure 4.3 The components of the release mechanism

5 The operation of release mechanism

5.1 The capacity of the mechanism

The development of smart systems able to control the overloading, requires the explicit definition of the release load. This load should correspond to an elastic deformation without causing any kind of damage in the components of the release mechanism. The release process should occur for a loading level close to, and not for a much lower, the value of the structural failure load. Otherwise the structure tends to be overdesigned.

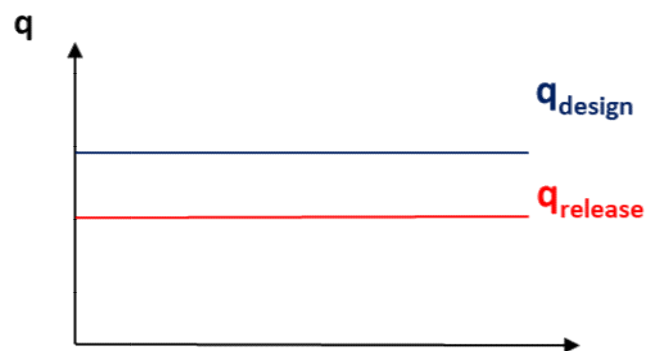


Figure 5.1 Schematic correlation between the design and the release load

The mechanism should not be able to operate under the wind load as calculated according to the EN 1991-1 [1]. Consequently, a specific range of loading should be defined for the mechanism to be activated and release the significant load of the accumulated snow. In Table 5.1, is presented the magnitude of the design snow load relative to the altitude for the Greek territory.

Table 5.1. Magnitude of the design snow load (kN/m^2)

Altitude A (m)		Zone A	Zone B	Zone C
from	to			
0	100	0.40	0.81	1.72
100	200	0.42	0.84	1.78
200	300	0.44	0.89	1.88
300	400	0.52	0.95	2.02
400	500	0.57	1.04	2.21
500	600	0.63	1.14	2.43
600	700	0.70	1.27	2.69
700	800	0.79	1.41	2.99
800	900	0.88	1.57	3.34
900	1000	0.99	1.75	3.72

It is proposed to define the upper release load limit as follows:

$$q_{release} = 0.50 \frac{kN}{m^2}$$

To ensure that the mechanism is activated at the aforementioned load level, its static behavior must be investigated and all the transfer mechanisms of loads, between the mechanism's components, understood. Due to the large displacements of the net under accumulated load, forces are exerted on the clip leading to its opening, as shown in Figure 5.2

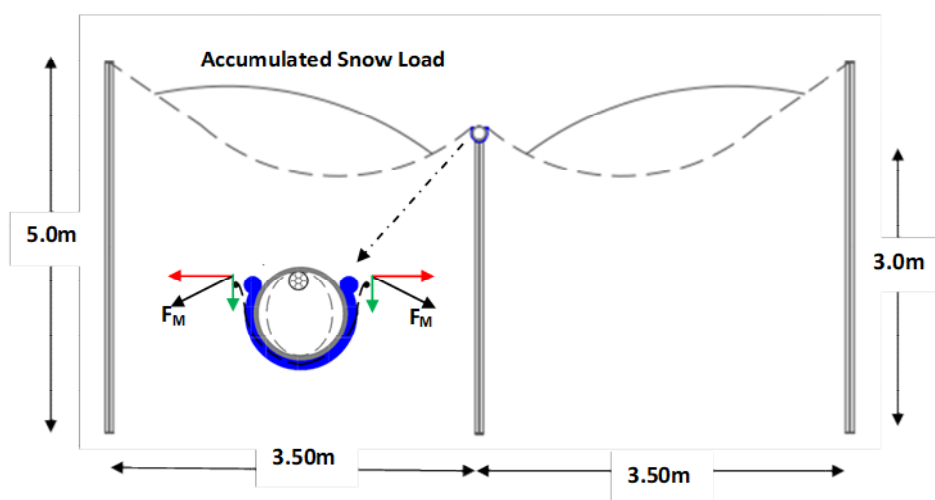


Figure 5.2 The deformed shape of the release mechanism

The design process of the mechanism includes the complete definition of the appropriate clip in terms of geometric configuration (diameter, thickness), so that it opens to the predetermined level load without inelastic deformations. The possible interaction of the clip with the pipe should be investigated and the influence of the slope of the roof must be evaluated taking into account the various distributions of the accumulated snow load. Therefore, the explicit definition of the release load is a multifactorial process and a careful approach to the phenomenon is required. For this reason, simulations of gradual complexity are created in an attempt to avoid significant errors in estimating of the release load. These simulations are presented in the following sections.

5.2 Simply Supported Model

In order to examine the static behavior of the release mechanism an initial finite element model in Ansys software is created. Basic assumption of this model is that the clip is considered pinned for the purpose of directly evaluating the resistance of the clip to the opening. A finite length ($w=100\text{mm}$) of the mechanism is examined taking into account the sloping nets on either side of it. The inclined length of the nets is 4 m , while the slope is under investigation as a critical design parameter. The net is modeled as shell elements, without bending stiffness (membrane behavior), with thickness $t=1.0\text{mm}$. Also, the clip is modeled with solid elements (8 nodes per element). Sensitivity analysis indicated that the appropriate mesh density of the clip is about 2.0mm . The lips of the clip are connected to the membrane via common finite element nodes (merge nodes). The model is presented in figures 5.3 and 5.4.

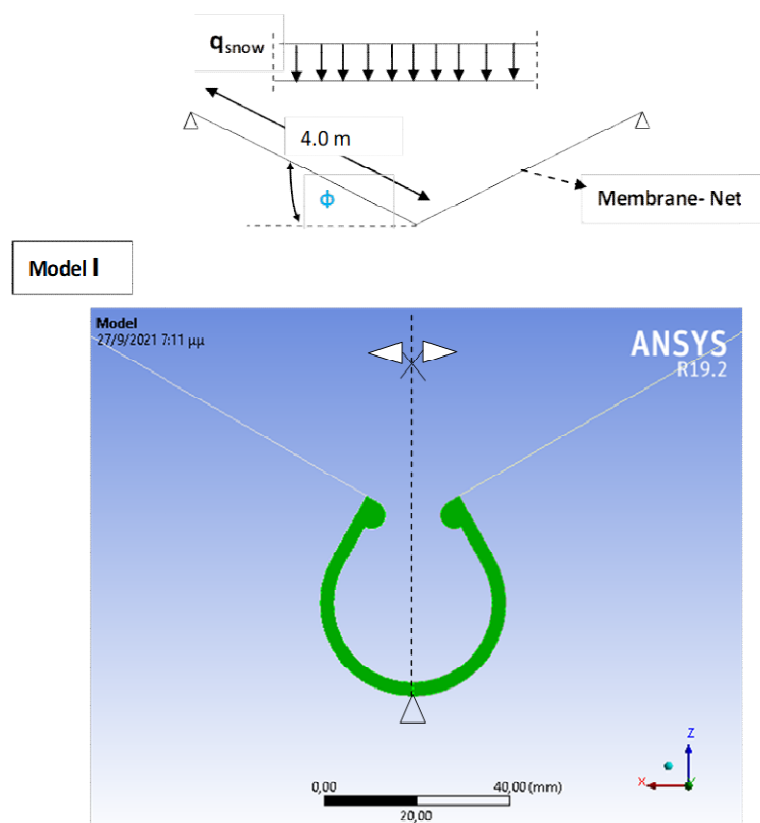


Figure 5.3 The symmetric simply-supported Model

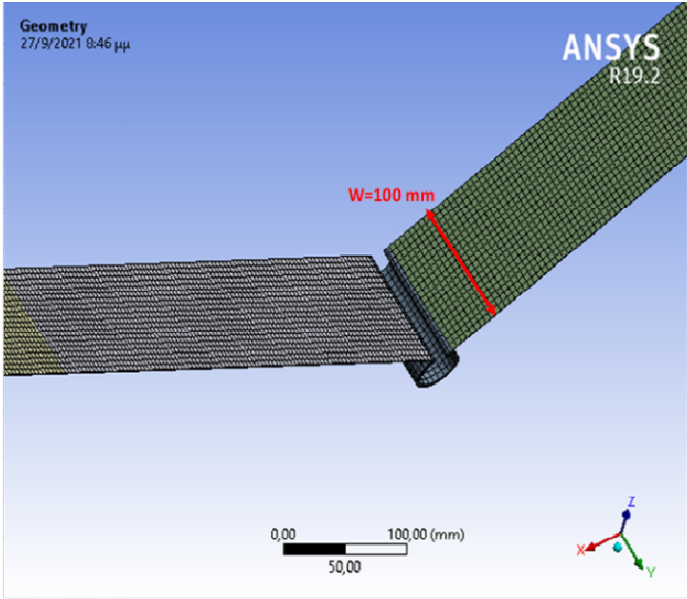


Figure 5.4 The perspective view of the Model

In this simply-supported model, it is necessary to define the release criterion. It is assumed that when the lips of the clip have been moved away from each other by a diameter (D) then the mechanism is activated. Due to the complete symmetry of the structural model, the release criterion can be expressed by the horizontal displacement of one edge of the clip. In figure 5.5, it is presented the full geometrical configuration of the clip that has been obtained through a repetitive process satisfying all the requirements as well as the release criterion in red.

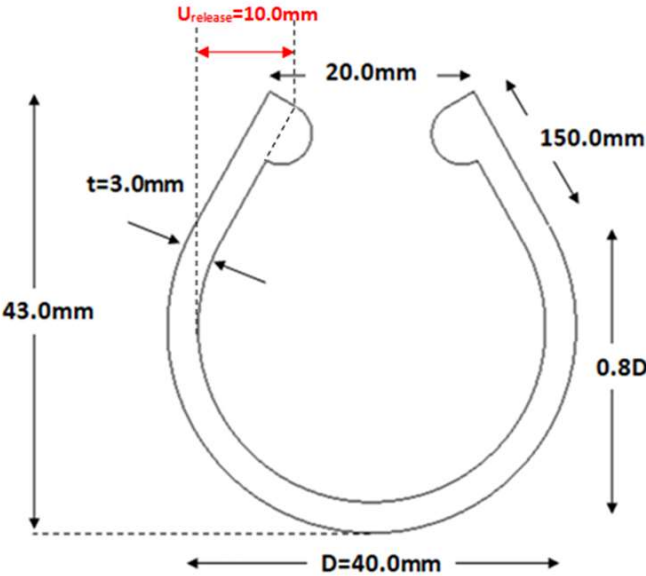


Figure 5.5 Geometrical configuration of the clip.

In the contexts of this thesis, the release mechanism is examined under snow loads with uniform distribution only and all results are obtained by means of geometric nonlinear analysis (large displacements).

Below are presented results for the clip of figure 5.6 and for initial slope of membrane $\varphi=30^\circ$. The release criterion is met when the load level reaches 0.59 kN/m^2 .

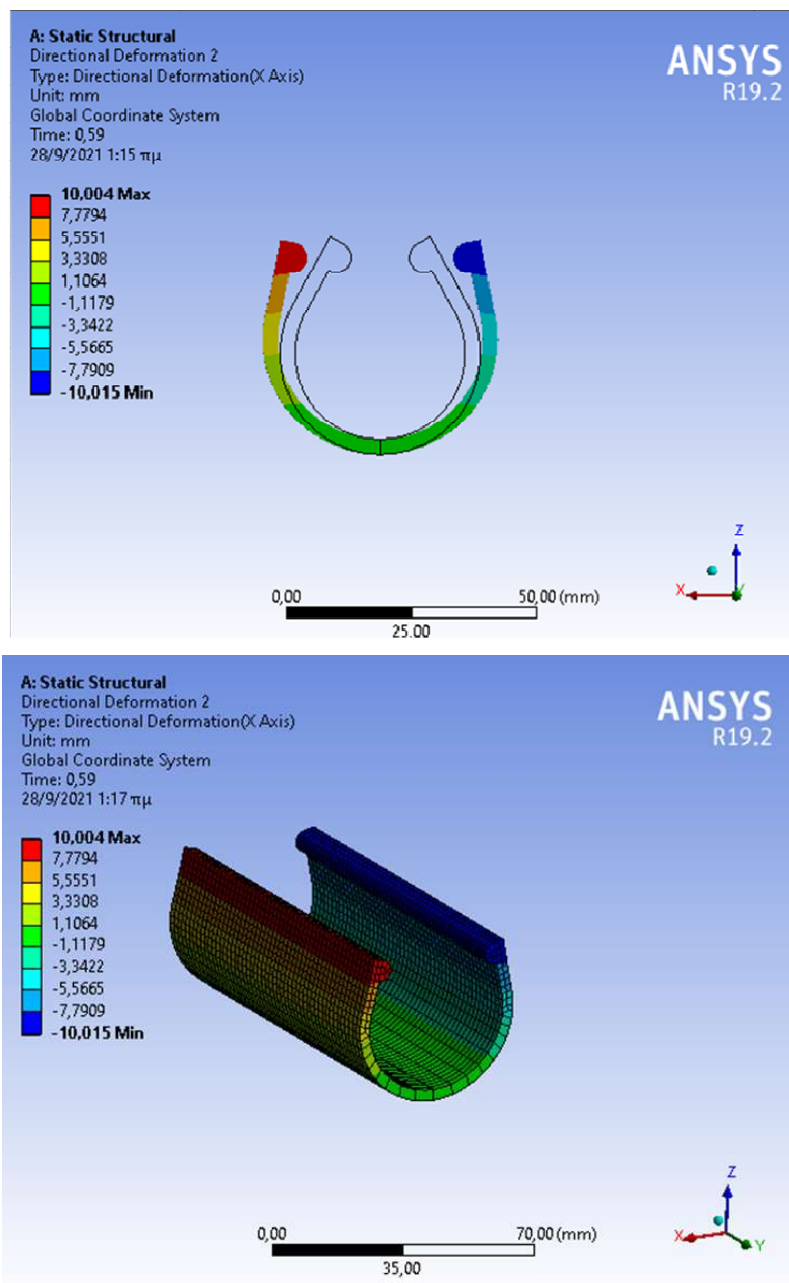


Figure 5.6 Directional deformation(x axis) of the clip at the moment of release.

In an attempt to control the release load, parametric analyzes are performed with clips of various geometrical characteristics. Keeping the thickness parameter constant, the influence of the diameter on all possible values of the roof angle (ϕ°) is under investigation. It is emphasized that each point of figure 5.8 has been emerged from a different analysis and signalizes the magnitude of snow load at which the release criterion is met. Clips with a diameter of 30, 40 and 50 mm are examined.

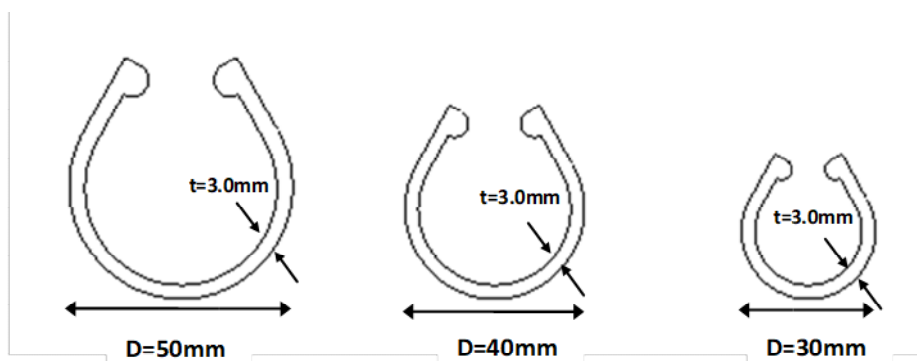


Figure 5.7 Geometrical configuration of the examined clips

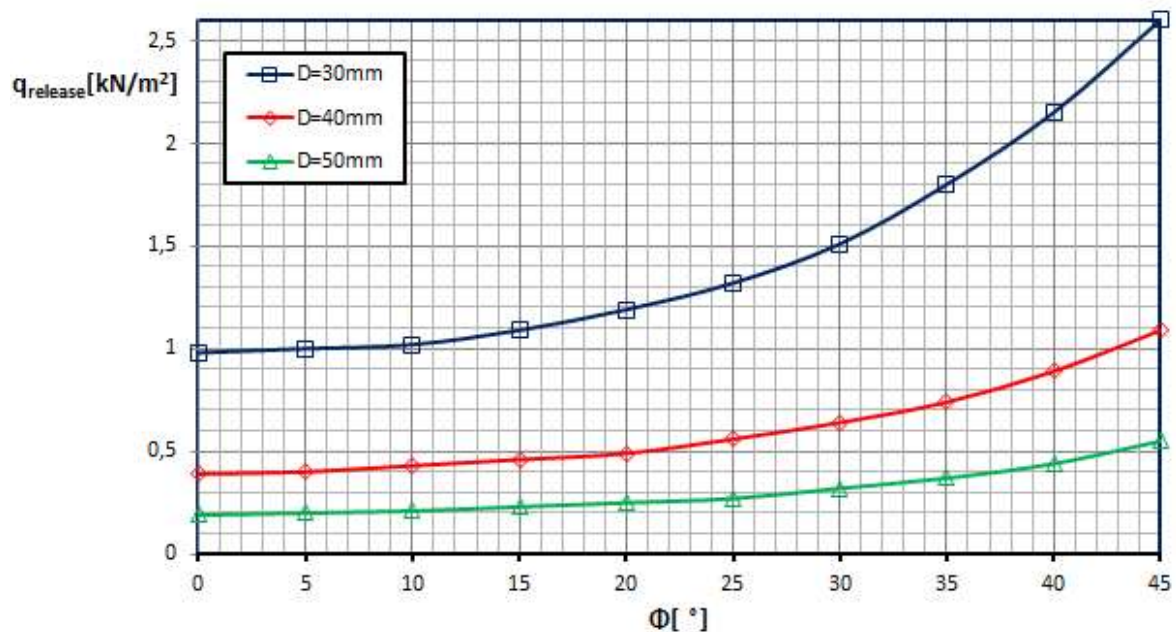


Figure 5.8. Spectrum of release load for all possible angles of nethouse roof

By increasing the diameter, the resistance of the clip to the opening is reduced and the corresponding release load [kN/m²] is lower. In addition, it is worth mentioning the increasing tendency of the release load as the initial angle of the roof increases. Remarkable result is that

the mechanism is just activated under the proposed limit load ($q = 0.50 \text{ kN/m}^2$), for diameter $D = 40 \text{ mm}$ (red line) and roof angle $\phi = 20^\circ$.

In the sequel, parametric analysis is carried out to evaluate the effect of the clip thickness on the release load, keeping the diameter constant, $D = 40 \text{ mm}$. Clips with uniform thickness $t = 2.5 \text{ mm}$ and $t = 3.0 \text{ mm}$ are investigated. Also, trying to define the optimal geometric configuration of the clip, its static behavior with a stiffener bottom ($t_{\text{bottom}} = 4.0 \text{ mm}$) is examined.

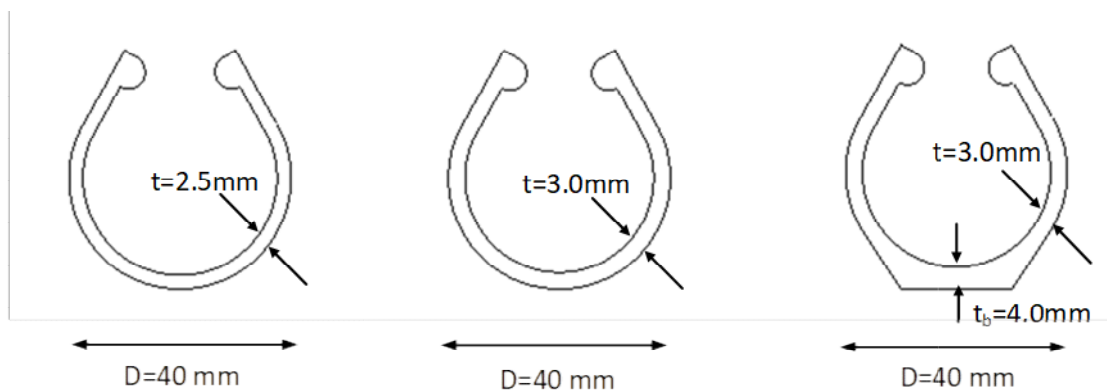


Figure 5.9. Geometrical configuration of the examined clips

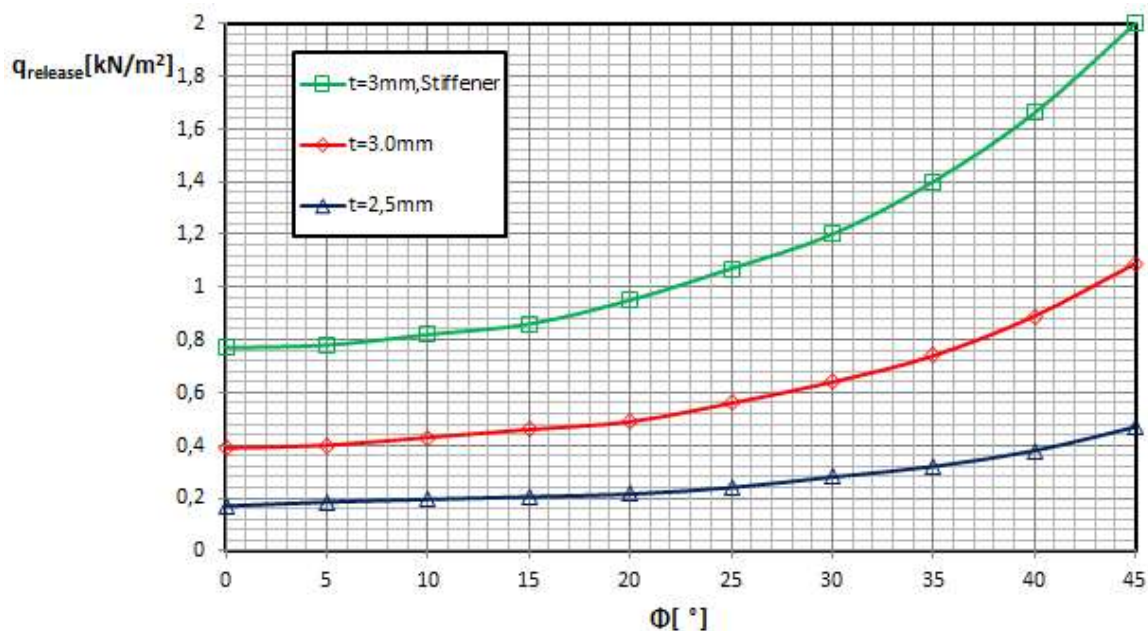


Figure 5.10. Spectrum of release load for all possible angles of nethouse roof

As the clip becomes stiffer, by increasing its thickness, the release of the mechanism occurs under a higher level of load. In particular, due to the symmetry, each leg of the clip behaves like a cantilever in terms of static engineering. Hence the maximum shear and bending

stresses are developed at the bottom of the clip. So, the local thickness of the bottom significantly affects the release load level as shown in diagram 5.10, comparing the green line ($t_{\text{bottom}}=4.0$ mm) with the red one ($t_{\text{bottom}}=3.0$ mm).

5.3 Contact supported Model

Contact problems are nonlinear and require significant computer resources to be solved. It is important to understand the physics of the problem and take the time to set up the model to run as efficiently as possible. In general, contact problems present two main difficulties. Firstly, the limits of the contact region are unknown until the execution of the simulation. Depending on the loads, boundary conditions and material properties, surfaces can come into and go out of contact with each other in an unpredictable and steep manner. Secondly, most contact problems are governed by friction. There are several friction laws, which all are nonlinear. Frictional response may be chaotic, making the numerical converge difficult.

The most simple and well-known algorithms for numerical modeling of the contact problems are based on penalty formulations. The penalty method uses a contact "spring" to establish a relationship between the two contact surfaces. The spring stiffness is called as contact stiffness. The elongation of the spring indicates the amount of penetration of one surface into the other.

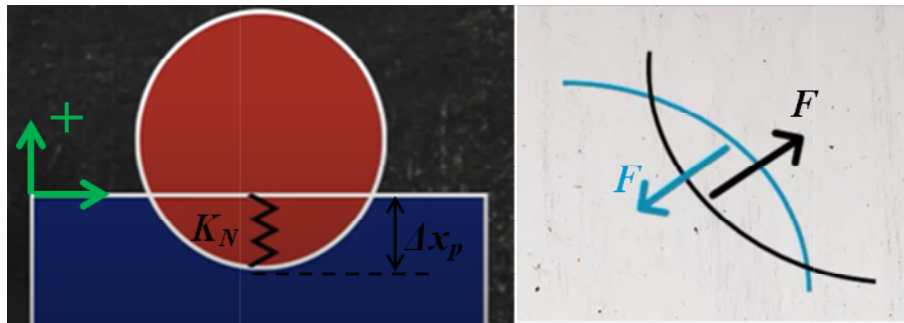


Figure 5.11 Formulation of Penalty Method regarding normal Stiffness

$$\{F\} = [K_N] \{\Delta x_p\} \quad (5.1)$$

Where K_N is the normal contact stiffness and Δx_p the amount of penetration. Mathematically the problem can be expressed as follows :

$$F = \begin{cases} 0, & \Delta x_p \geq 0 \\ K_N \Delta x_p, & \Delta x_p < 0 \end{cases} \quad (5.2)$$

This equation means that only when one surface penetrates the other, the force transfer through contact is possible. It is worth mentioning that penetration is a numerical tool for simulating the transfer of forces through contact and does not correspond to reality. Hence, its amount should be controlled and minimized. In addition, the penalty method requires the determination of the tangential \mathbf{K}_t contact stiffness. The amount of slip in sticking contact depends on the tangential stiffness as follows :

$$\tau_i = \begin{cases} K_t v_i, & \|\tau\| = \sqrt{\tau_1^2 + \tau_2^2} - \mu P \leq 0 (\text{Sticking}) \\ \mu P \frac{\Delta u_i}{\|\Delta u_i\|}, & \|\tau\| = \sqrt{\tau_1^2 + \tau_2^2} - \mu P = 0 (\text{Sliding}) \end{cases} \quad (5.3)$$

Where

- τ_i : τ_1 and τ_2 , Friction in direction 1,2 (figure 5.12)
- μ : Coefficient of friction
- P : Force perpendicular to contact face
- Δu_i : Slip distance in direction i

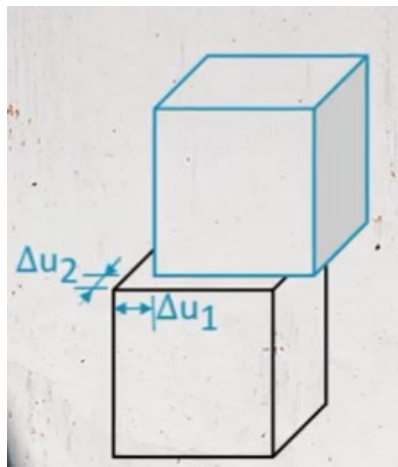


Figure 5.12. Slip distance between contact pair

In Figure 5.13, the standard and the modified Coulomb friction laws are presented. The first model is well known in the engineering community but it is not efficient for an interface problem with deformable bodies. One of the weaknesses of the Standard Coulomb modeling is induced by the fact that the relationship between sliding displacement and the tangential load is discontinue. To overcome this difficulty, it is quite usual to regularize the Coulomb friction law which is mathematically described in equation 5.3.

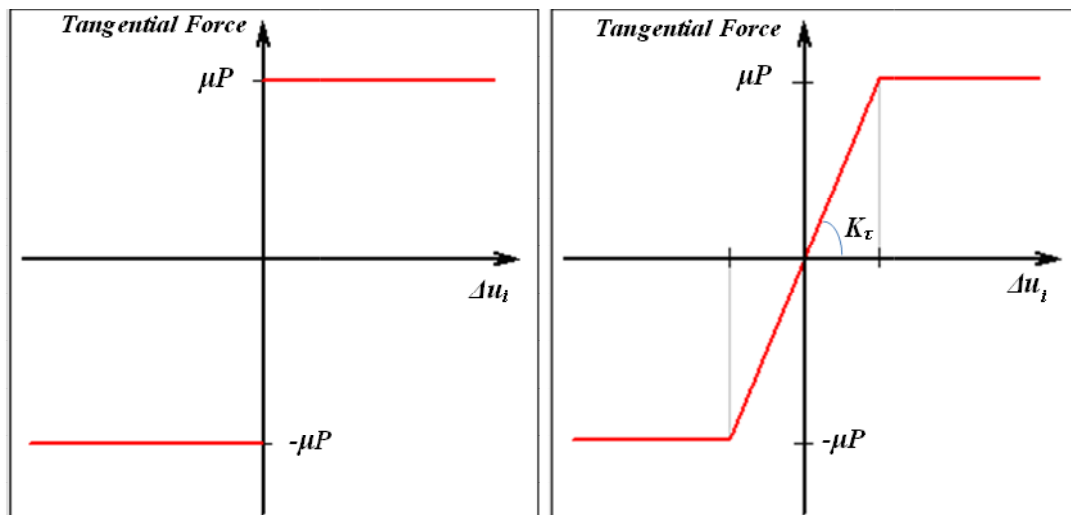


Figure 5.13 Standard Coulomb and modified Coulomb friction models

In general, higher stiffness values (K_N, K_τ) decrease the amount of penetration/slip, but can lead ill-conditioning of the global stiffness matrix and to convergence difficulties. Lower stiffness values can lead to a certain amount of penetration/slip and produce an inaccurate solution. Ideally, it should be defined a high enough stiffness that the penetration/slip is acceptably small, but a low enough stiffness that the problem will be well-behaved in terms of convergence. Ansys provides default for contact stiffness (K_N, K_τ), allowable penetration (FTOLN) and allowable slip (SLTO).

In an attempt to more realistically simulate the problem, a finite element model of the mechanism in the presence of the deformable plastic pipe is created. In the simulation, the main components of the mechanism, clip and plastic pipe, are connected via contact elements. In a surface contact analysis in Ansys software, it must first be designate the target (master) and the contact (slave) surface. In case that both bodies of the contact pair are flexible, the choice of which surface is designated as target or contact can cause a different amount of penetration and thus affect the solution accuracy. Designation of contact surfaces depends on the shape, dimensions, mesh, stiffness and type of elements. In our case, contact surfaces meshing and bodies stiffness both tend to be similar. However, it is expected that the concave surface of the clip comes into the convex surface of the pipe, a situation that according to FEA guidelines (Ansys) determines pipe as target (master) and clip as contact (slave).

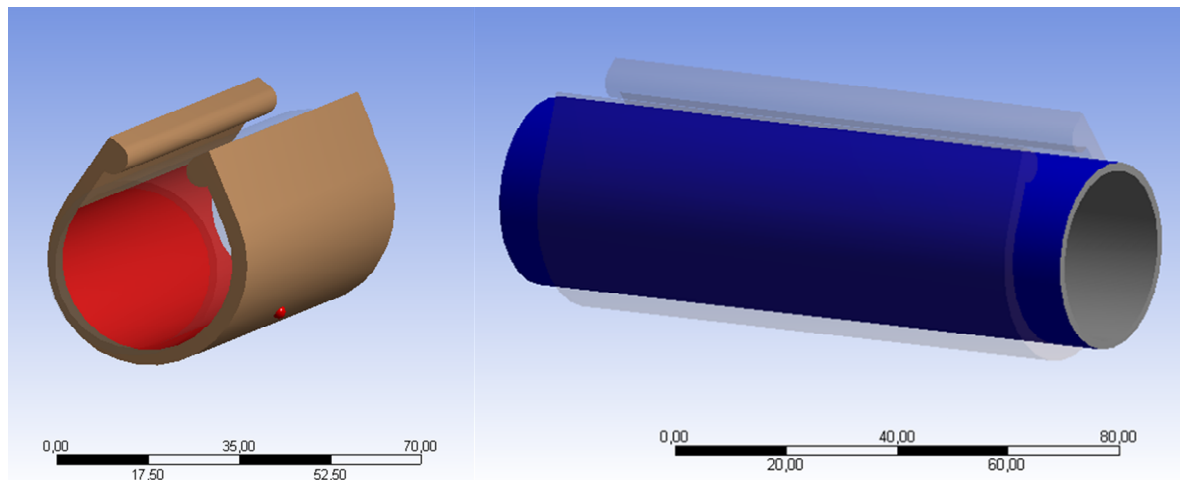


Figure 5.14. Contact Surface (pink) and target surface (blue)

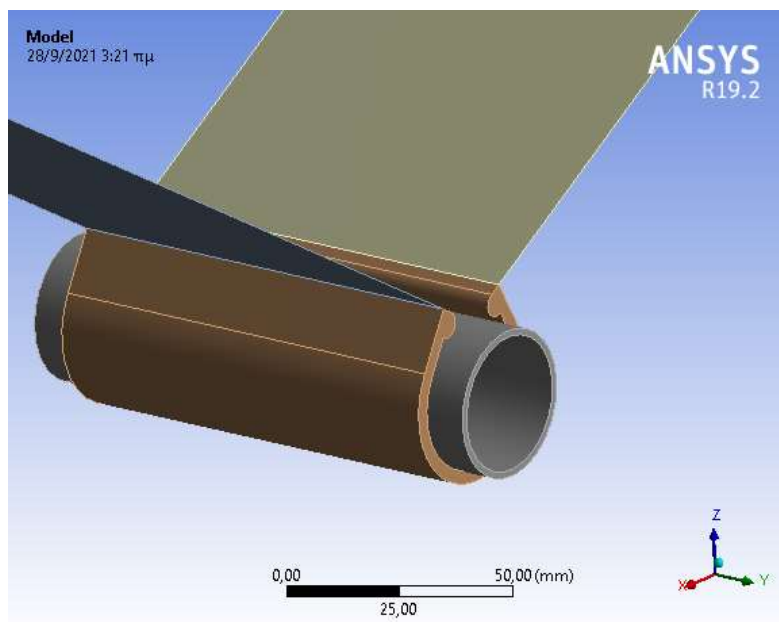


Figure 5.15 Set up of contact supported Model

For this advanced contact model, the criterion for activating the mechanism and releasing the accumulated snow load is defined as the loss of contact between the lowest points of the pipe (Point B, figure 5.16) and the inner surface of the clip. As the vertical load of snow is increased incrementally, the gap between the components of the release mechanism at its characteristic points is recorded to identify its mode of operation and predict the limit release load. Characteristic points are defined the A and B as shown in Figure 5.16.

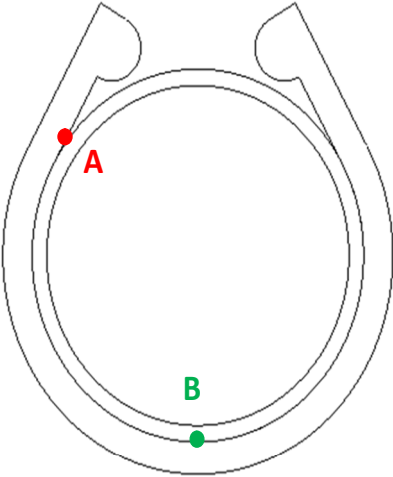


Figure 5.16 Definition of characteristic points A and B.

In the case of an initial angle of inclination of the membrane equal to 30° , the gap recordings between the release mechanism components at points A and B are plotted in the figure 5.17. The examined mechanism consists of a clip with diameter $D = 40 \text{ mm}$ and thickness $t = 3.0 \text{ mm}$ and its exact geometric description is given at figure 5.5.

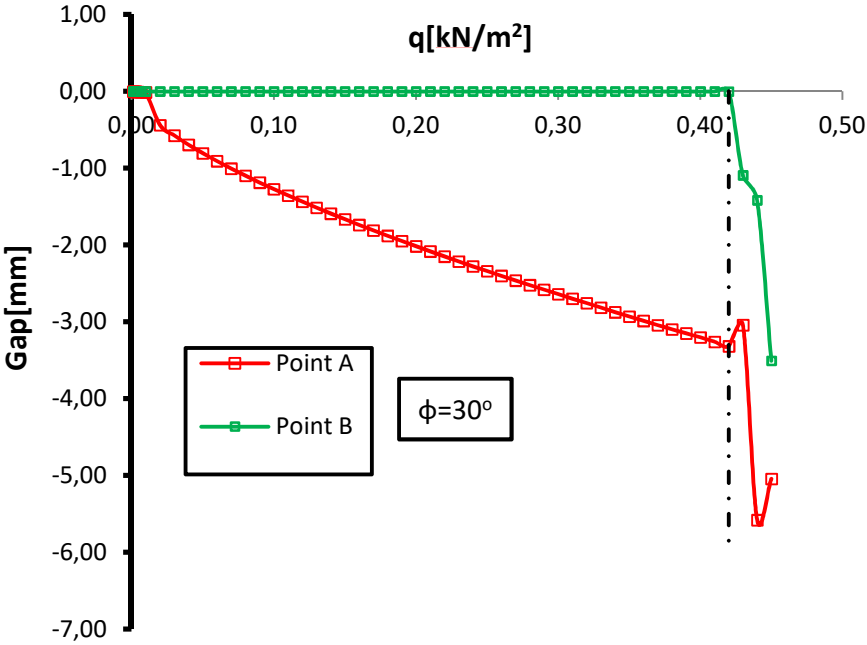


Figure 5.17 Definition of characteristic points A and B.

It is observed that the loss of the contact occurs from the beginning of the analysis in point A, while point B is the last point of contact before the release of the mechanism.

Consequently, the release criterion is met when the load level reaches 0.42 kN/m^2 . It is worth mentioning that the identical pinned-supported model provides a higher load release value up to 0.59 kN/m^2 . This discrepancy is evaluated and discussed furthermore in the next subsection.

Investigating the influence of the friction in the certain contact problem, analyzes with several values of friction coefficient (μ) are carried out. The friction law used is the modified Coulomb. The results indicate that the operation of the mechanism is not governed by friction as it was initially expected. This mainly occurs due to the absence of net between pipe and clip in the finite element model and the resulting friction that would be generated as is the case in the real situation. In figure 5.18, the influence of magnitude of friction coefficient on the response is shown. Analyzes are performed with two extremely values of the friction coefficient.

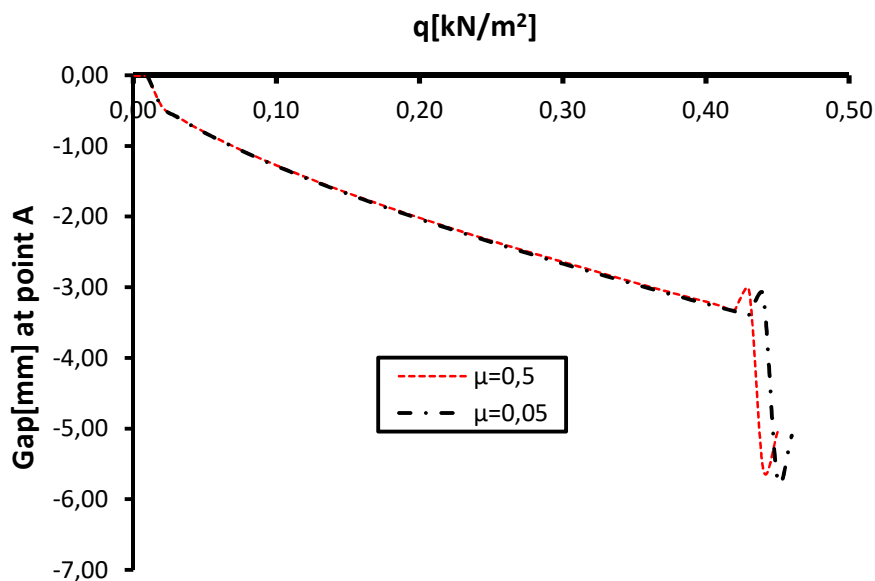


Figure 5.18 The influence of magnitude of friction coefficient on the response

During the contact analysis, the penetration between the contact pair should be assessed in order to understand the transfer mechanism of forces between the bodies. By stretching the clip, its lowest point comes up and penetrates the pipe. The force that is transmitted is the vertical component of the membrane force of the inclined net. In figure 5.19, the penetration amount at point B as the vertical snow load $q(\text{kN/m}^2)$ increases for several angles of inclination of the membrane is presented. It is observed that, as the initial angle $\varphi(^{\circ})$ of the roof increases, the penetration between the components of the mechanism and the

corresponding release load are higher. The points of intersection between the curves and the horizontal axis indicate the release load as the contact is lost (zero penetration).

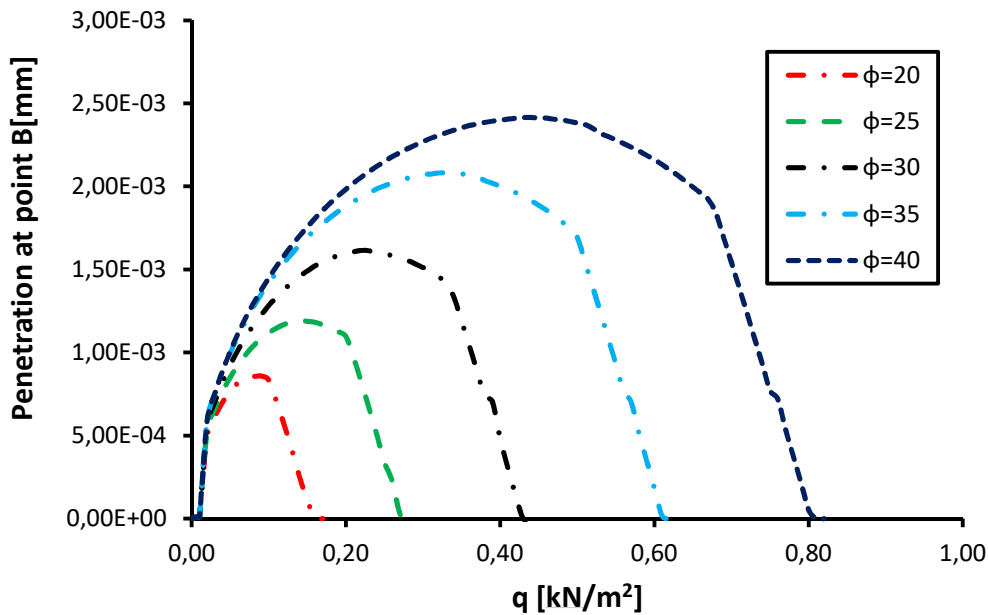


Figure 5.19 The amount of penetration for several angles of inclination of roof

5.4 Von mises Stresses of the clip

It is essential to ensure the ability of reassembly of the mechanism after the release. This presupposes the limitation of the developing stresses in the clip below the material yield limit, until its opening. The clip is made of PVC and the yield limit $f_y = 55 \text{ Mpa}$ is taken into account. It is considered that the appropriate failure criterion is the Von mises which combines normal and shear stresses and it is expressed as follows :

$$(\sigma_{xx} - \sigma_{yy})^2 + (\sigma_{yy} - \sigma_{zz})^2 + (\sigma_{zz} - \sigma_{xx})^2 + 6(\tau_{xy}^2 + \tau_{yz}^2 + \tau_{zx}^2) = 2f_y^2 \quad (5.4)$$

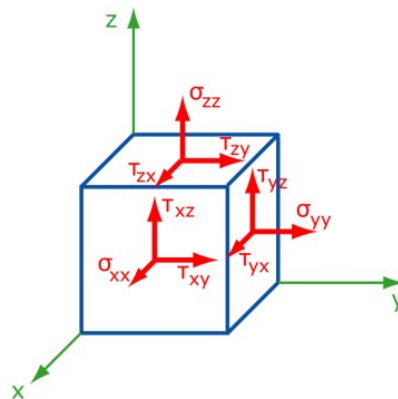


Figure 5.20 Normal and shear stresses

At the release moment, the maximum von mises stresses value is displayed at the bottom of the clip and is equal to 42.3 Mpa. Therefore, the mechanism remains elastic with a material exploitation factor $a=0.75$.

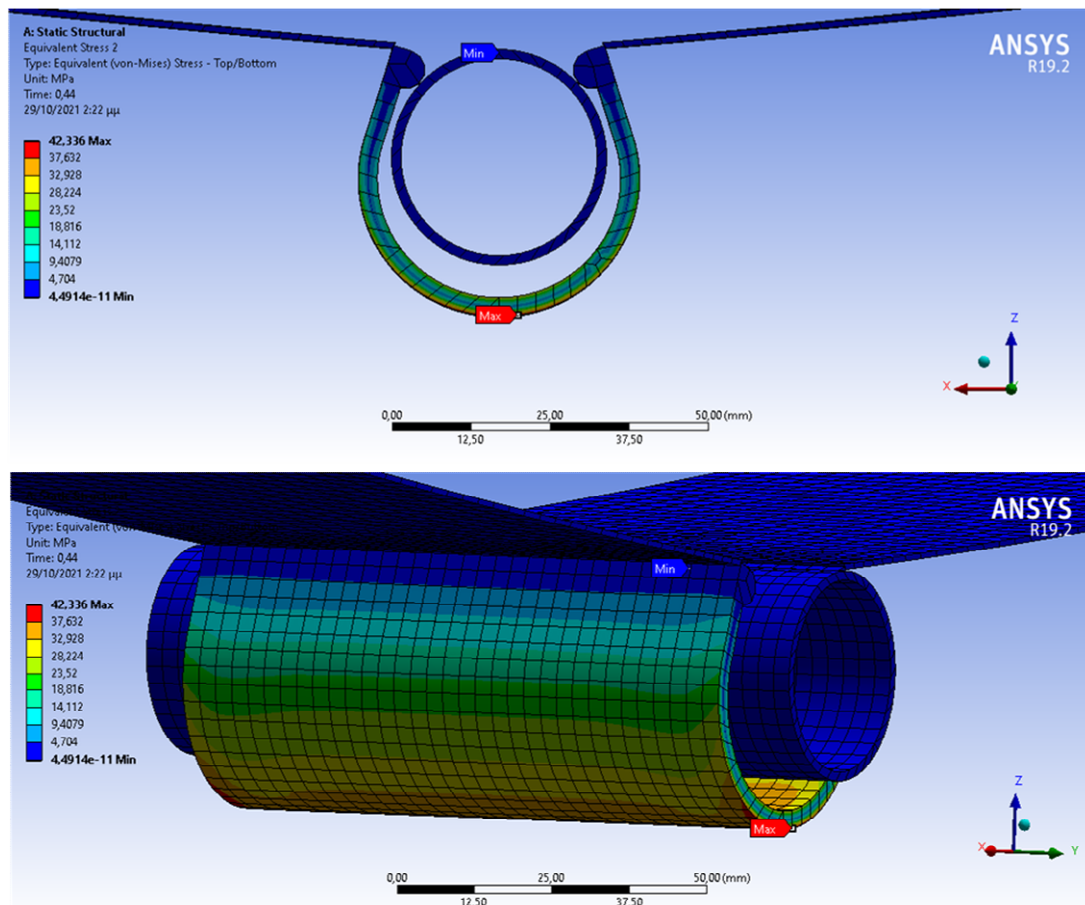


Figure 5.21 Von mises stresses

5.5 Comparison of models

In order to form an accurate and direct way to define the release load, results of both models should be compared. Through this process, the pros and cons of each model may be emerged. A proper study approach of a physical problem should start with a simple modeling and its complexity should be gradually increased by improving its initial rough assumptions. Therefore, the pinned supported model is initially examined and afterwards the most complex supported contact one.

First, the simply supported model is discussed. It is reminded that the release criterion is met when the horizontal displacement of each lip of clip exceeds half of its diameter. The main weakness of this model is induced by the fact that the vertical component of the

membrane force is directly transferred to the pinned support. Due to the effect of large displacements, this force component tends to intensively stretch the clip, contributing to its opening. Thus, omitting the effect of vertical force component, the release load of mechanism is overestimated. Nevertheless, the influence of this vertical force on the release mechanism is clearly less than that of the horizontal.

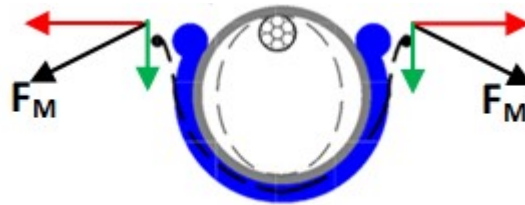


Figure 5.22 The force components of the net attached on the clip

In the complicated contact model, the release occurs when the contact between the components (clip, pipe) of the mechanism is lost. In terms of numerical approach, a simple release criterion has been established which considers that when the contact at the bottom of the pipe is lost then a complete release takes place. As the snow load increases, the initial angle ϕ reduces so does the vertical force (F_z) as shown in figure 5.23. The presence of this force ensures contact between the components of the mechanism. At the moment when the net becomes horizontal F_z is eliminated and the contact is at stake (Fig 5.24).

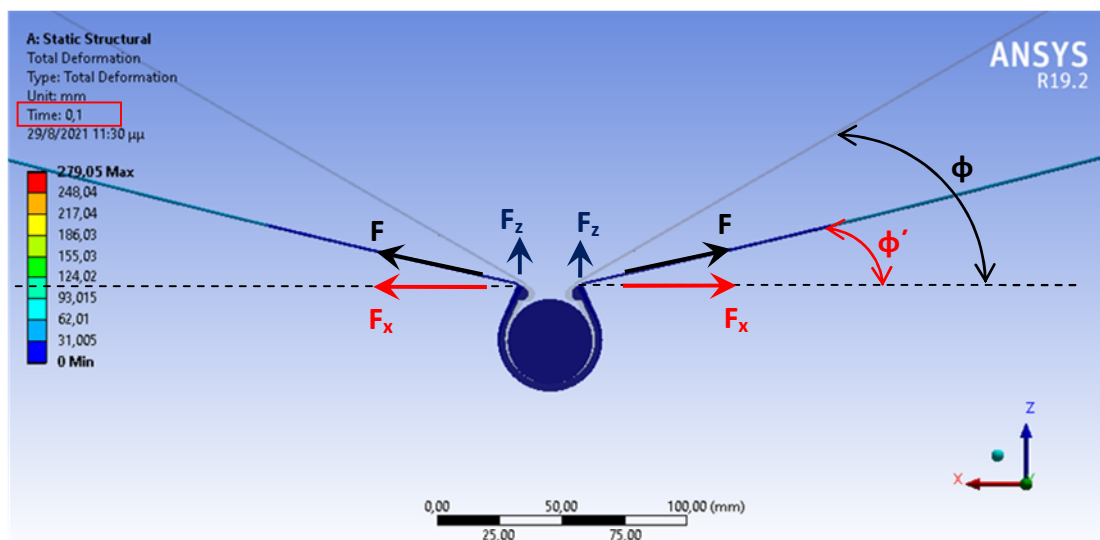


Figure 5.23 The components of the force at a random angle (ϕ') of the membrane.

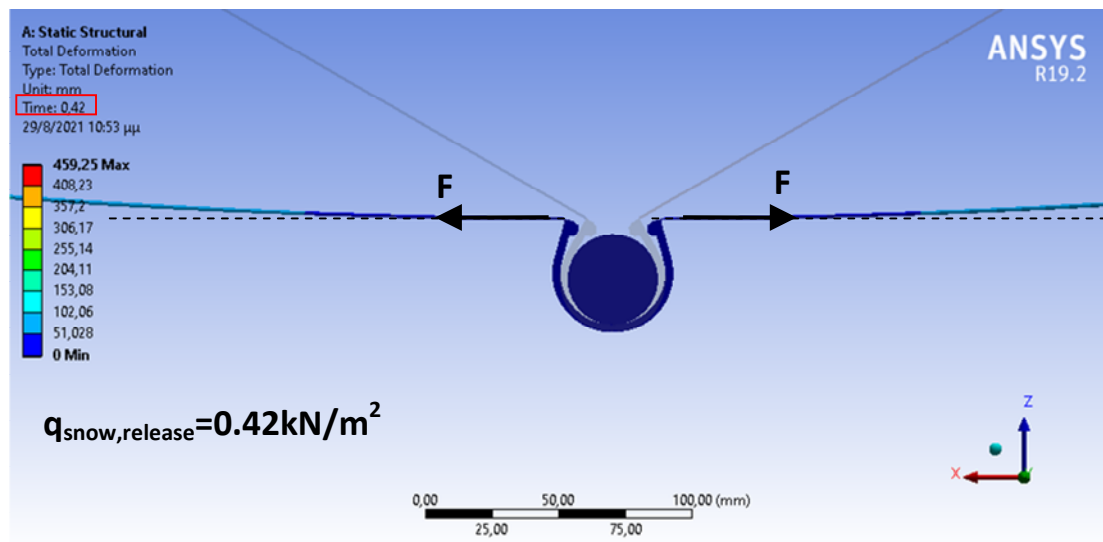


Figure 5.24 The frame of the release moment

However, the aforementioned criterion does not fully correspond to reality. In particular, the mechanism is not certain to open if contact is lost at point B (Fig 5.16), as this may occur without the opening of the clip lips being sufficient enough to separate it from the pipe. The clip is now hanging from the pipe and therefore the contact still exists but it is present to the upper part of clip (Fig 5.25). Consequently, this model tends to underestimate the real release load of the mechanism.

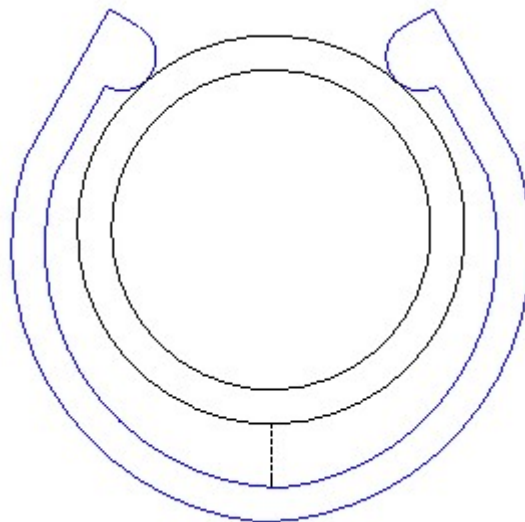


Figure 5.25 The new contact position

This kind of contact, given in Figure 4.25, is a subject of an ongoing research where a significant computational effort is required. In an advanced approach, more efficient model algorithms must be used which will be able to simulate the instantaneous contact loss between

the components without interrupting the analysis, providing the actual load level, under which the mechanism is released

For the clip with the geometric configuration as presented in figure 4.8, both structural models were executed for several initial net angles. Quoting the results in the same chart, an overall view of the differences between the two models is composed. The exact values of the actual release points are included into the area bounded by the curves corresponding to each model. The requirements of both criterion tend to converge as the angle φ increases.

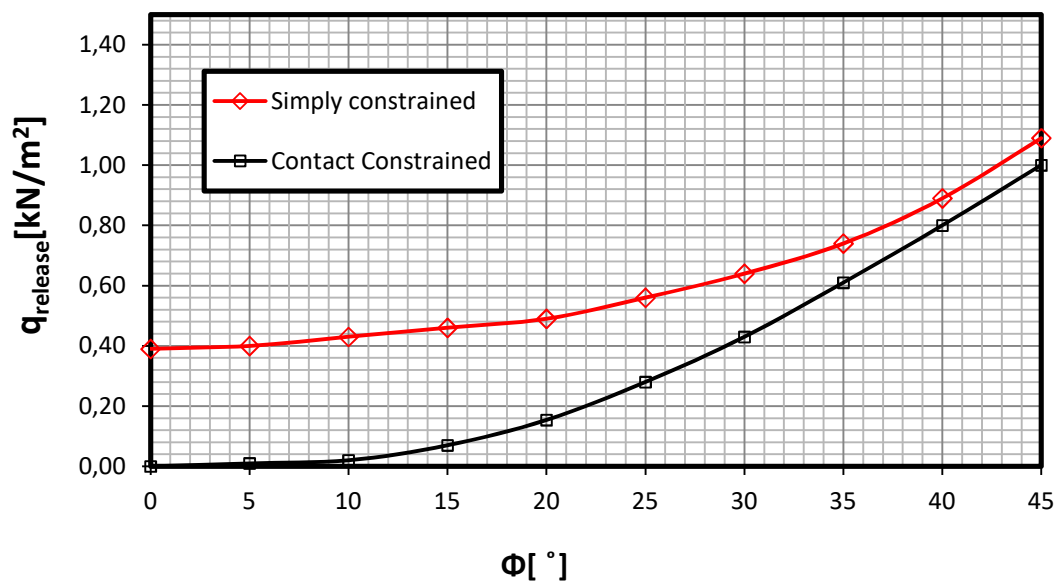


Figure 5.26 Comparison of the simply and contact supported Model

Figure 5.27 shows the horizontal displacements of the clip lips that are obtained by means of the contact supported model for a range of net angles. In case of slope angle $\varphi = 30^\circ$, the contact model indicates a release load at $q = 0.42 \text{ kN/m}^2$. At that time, the lip of the clip has been deformed by 7.5 mm, 25% less than the required release displacement of the first model. Through this example, the quantification of the discrepancy between the two release criteria is emerged. Again, this deviation is limited by increasing φ angle, as previously observed in Figure 5.26.

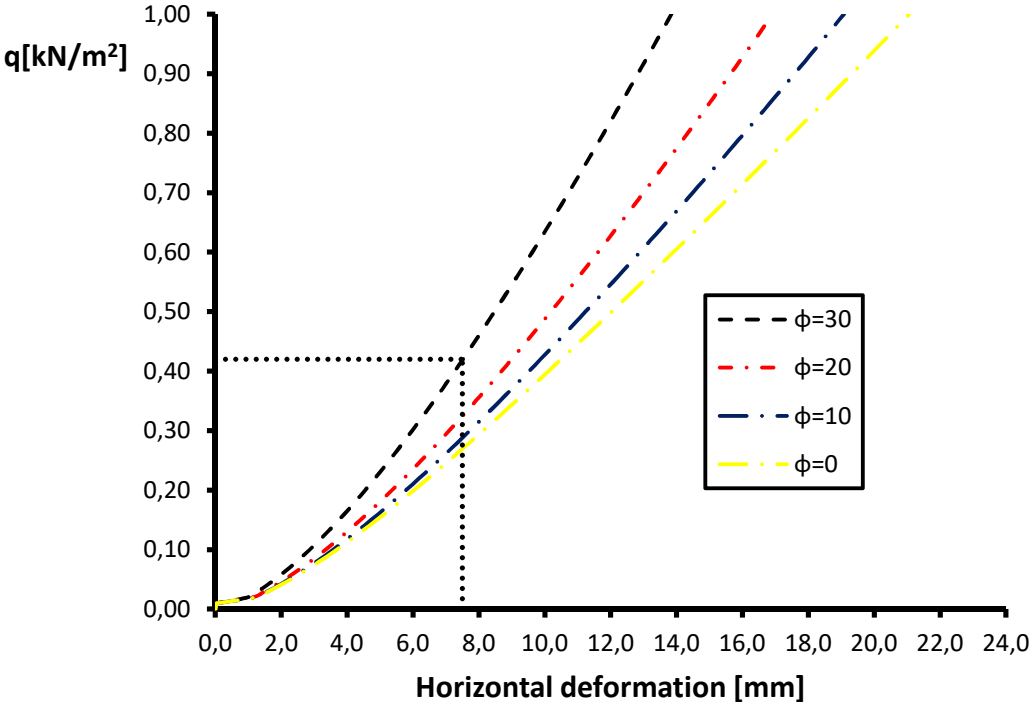


Figure 4.27 Equation paths obtained by means of contact supported model

6 Further Investigation

6.1 Full scale experiment

In order to evaluate and calibrate the numerical models, experimental full scale tests of nethouse structure will be carried out. The tests will be performed in the Institute of Steel Structures, NTUA, examining a real case of a tensile structural system for nethouse. The concept is to investigate the response of the structure under vertical loads that simulates the snow load. The test structure consists of three panels with dimensions 2m x 4m each and its height is approximately 1.60 m. Concerning the path of loads, it should be mentioned, that the agricultural net is supported to cables. These main cables are suspended from steel columns and restrained by sloping anchored cables. The angle of the restraining cables is 25°. Prestressing is established into the system as described in section 3.2.

The main experimental set up (net, cables, columns) is placed on a complex of cross steel beams lying on the floor (figure 6.1). On the longitudinal beams (SHS 140x140x5, red ones in figure 4.28) the columns are supported and the restraining cables are anchored. Also, transverse beams (RHS 200x100x10, blue ones in figure 6.1) are arranged below the longitudinal ones, stabilizing all the structure as they are anchored to the strong laboratory floor (thickness slab=2 m).

It is noted, that the structural behavior of the system will be tested for two different slopes of the net roof. Firstly, the experiment will be performed with the flat configuration of the roof and secondly with the duopitch one. The layout of the experiment has been designed in such a way that, through a simple modification, the slope of the roof can be adjusted. The duopitch setup is formed with an inclination angle equal to 20° and only two panels need to be loaded for the corresponding experiment (fig 6.4). In this layout, the release mechanism, as described in detail in the previous chapters, is going to be attached. In figures 6.1, 6.2 and 6.3 the experimental setup of flat nethouse is presented. While, in figures 6.4, 6.5 the experimental setup of duopitch nethouse is pictured.

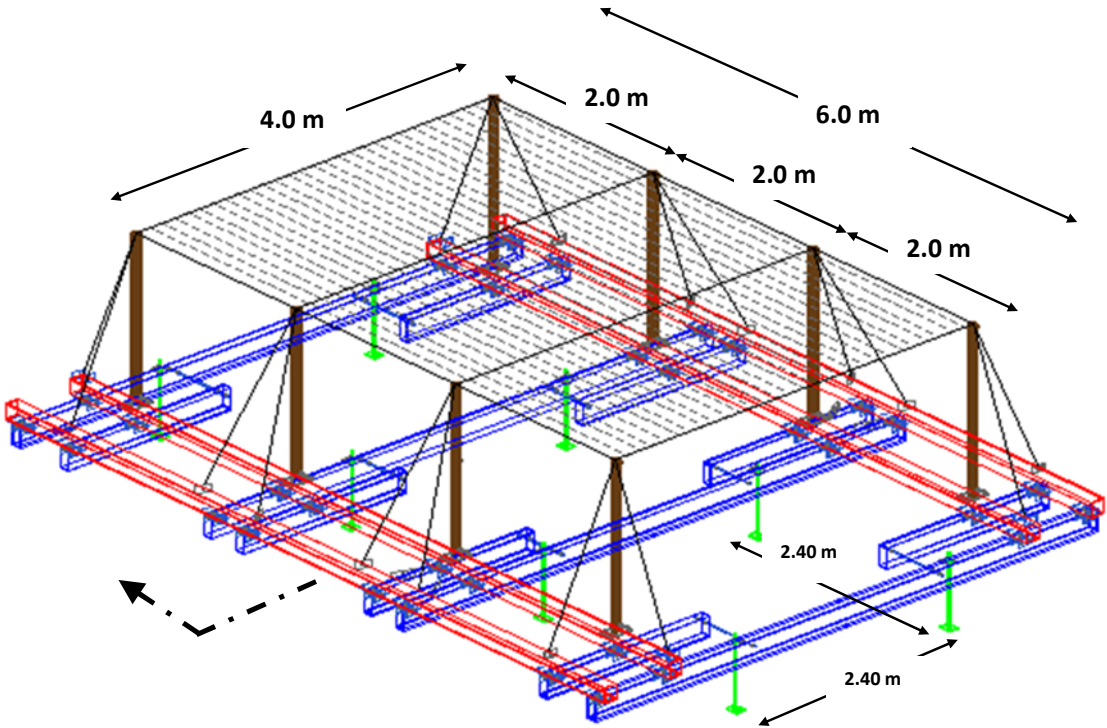


Figure 6.1 Experimental setup of flat nethouse – Perspective view

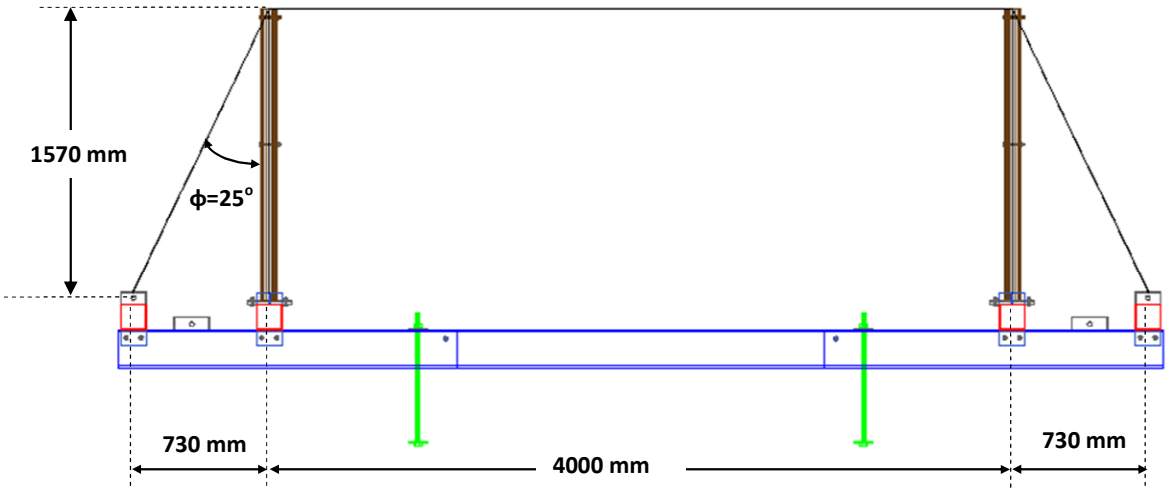


Figure 6.2 Section of flat nethouse

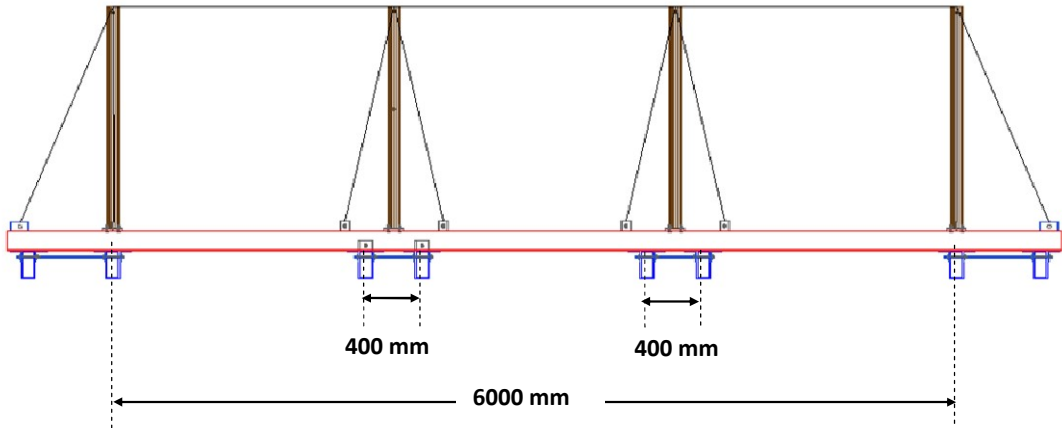


Figure 6.3 Facade of flat nethouse

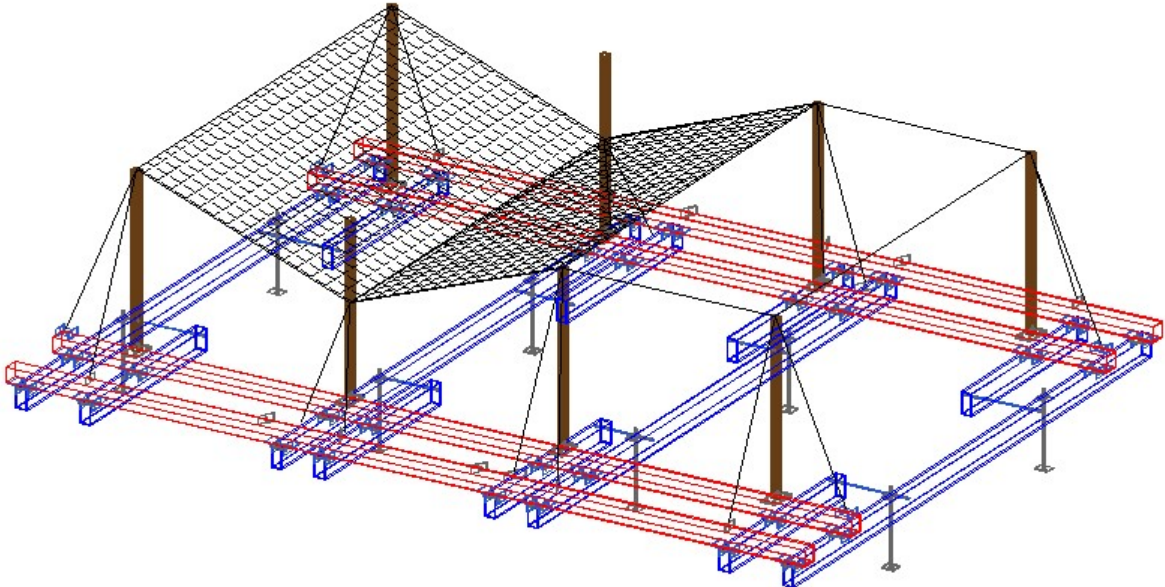


Figure 6.4 Experimental setup of duopitch nethouse – Perspective view

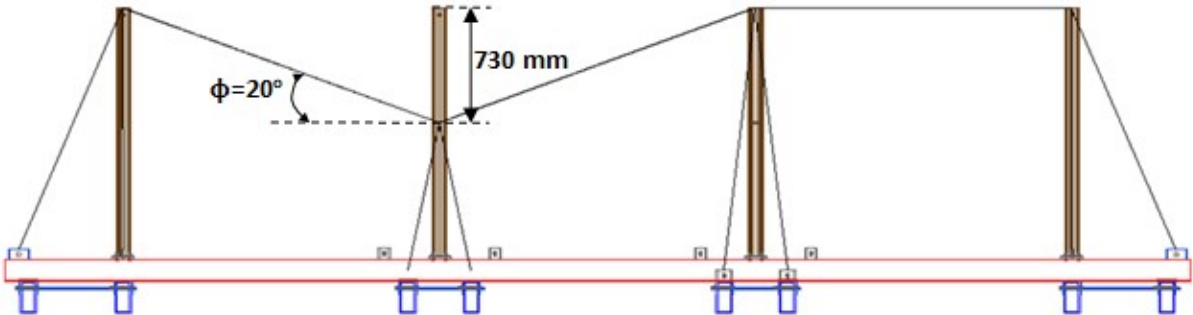


Figure 6.5 Facade of duopitch nethouse

The experimental steel cross sections in Tables 6.1 and 6.2 are listed below.

Table 6.1 Experimental hollow steel sections


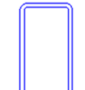

Auxiliary substructure	SHS 140x140x5	
	RHS 200x100x10	
Column	CHS 88.9x4	

Table 6.2 Experimental cable sections

Cables	Suspension $\Phi 20$	
	Restraining $\Phi 10$	

In many cases, imposing a uniformly distributed load experimentally may be a challenge. This problem becomes even more complicated in the case of an extremely flexible surface such as a agricultural net. In the contexts of this experiment, sawdust/wood shavings are selected for the implementation of the uniformly distributed load. The sawdust, as a bulk material, can follow the large deformations of the flexible surface of the net, maintaining the required loading conditions.

The density of snow varies depending on the prevailing weather conditions and the time interval it remains on a surface. For settled snow, the unfavorable possible scenario, specific gravity ranges from 2 kN/m^3 to 3 kN/m^3 . The specific gravity of the selected sawdust, takes the value of the 2.1 kN/m^3 which is close to the aforementioned corresponding range of snow. For the needs of the experiment the load level reaches up to 0.50 kN / m^2 in total and it will be imposed incrementally in three steps.

The main measurements of the experiment will be the total vertical deformation of the agricultural net, under the predefined load level, the tension in the cables and the release load of the mechanism.

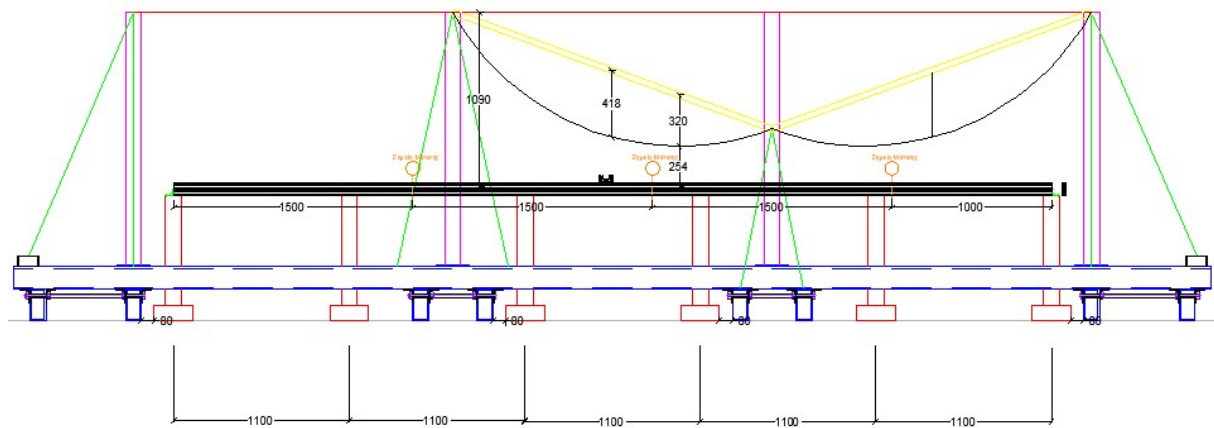


Figure 6.5 Facade of duopitch nethouse with monitoring systems

6.2 Deformed shape of roof-Ponding

During heavy snowfalls the structure may develop deflections such that a downward slope becomes reversed. This can produce what is generally referred as ‘ponding’ (Figure 6.6, Figure). Due to the flexibility of the membrane, the accumulation of snow or hail leads to larger deflections and as a consequence further attraction of load is allowed. There is a higher perceived risk with structures covered with smooth surface materials (such as the plastic nets). Large loads of snow can be experienced in membrane structures and for this reason ponding must be avoided. The risk of ‘ponding’ in such structures during the summer period should also be taken into account, as hailstorms may often occur, after a period of rather high temperatures.

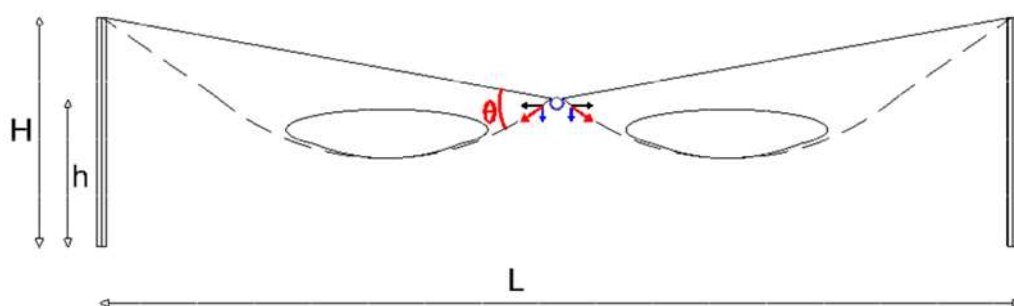


Figure 6.6 The deformed shape of the roof under the accumulated load

As the load accumulates, the angle θ ($^{\circ}$) shown in Figure 6.6, increases. The development of an integrated methodology for the release mechanism should quantify the phenomenon of ‘ponding’. Therefore, many load distributions have to be considered taking into account both the ponding and the randomness of the snow. Thus, the limit load can be defined with safety and the crop will not be in danger during the post-release phase



Figure 6.7 The deformed shape of the roof under the accumulated load

7 References

1. Brian Forster, “The European Design Guide for Tensile Surface Structures”,2004
2. Charis J. Gantes, Konstantina Koulatsou, Methodology for Nonlinear Finite Element Analyses to Evaluate Strength of Steel Structures, Institute of Steel Structures, National Technical University of Athens, Athens, Greece
3. Diego Orlando, Nonlinear Dynamics and sensitivity to imperfections in Augusti’s Model
4. D. Briassoulis, A. Mistriotis, D. Eleftherakis, Mechanical behaviour and properties of agricultural nets—Part I: Testing methods for agricultural nets, Agricultural University of Athens, Department of Agricultural Engineering,
5. Katie Jo Engle, Study on Physical and Mechanical Properties of Agricultural Netting Products, Iowa State University
6. Sergio Castellano, Design and use criteria of netting systems for agricultural production in Italy
7. Johan Blaauwendraad, “Ponding on light-weight flat roofs: Strength and stability” Delft University of Technology, The Netherlands
8. Johan Blaauwendraad, “Ponding on flat roofs : A different perspective”, Delft University of Technology, The Netherlands
9. CEN, “EN 1991-1-3: Eurocode 1: Actions on structures – Part 1-3: General actions – General actions -Snow loads,” 2005.
10. CEN, “EN 1991-1-4: Eurocode 1: Actions on structures – Part 1-4: General actions – Wind”

8 Annex A/ Primary experiments of release mechanism

Tensile tests were performed for the innovative release mechanism by using an INSTRON testing machine/Model 5900 (Figure 1) at the facilities of the Laboratory of Farm Structures (AUA, Athens). The aim was to investigate the interaction between the components of mechanism (clip, pipe, net) and define the limit load of the release mechanism in each case.

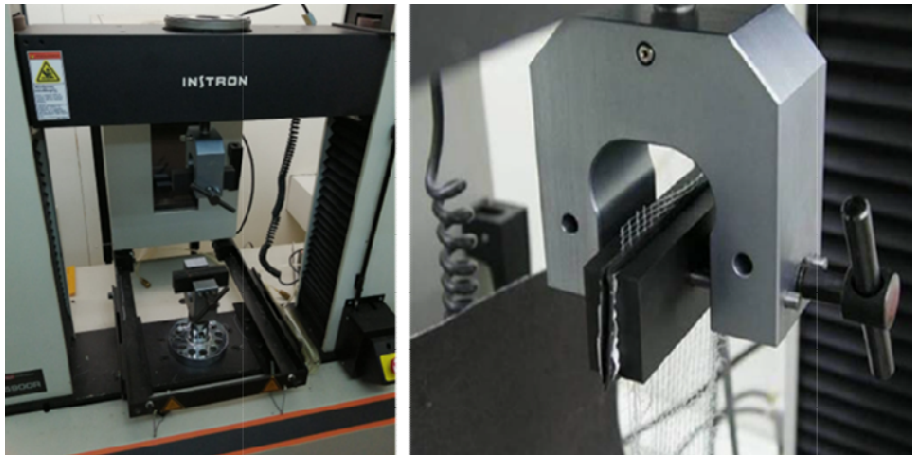


Figure 1.The tensile machine Instron 5900 with specially designed grips

The concept of the experiment was to examine the behavior of the release mechanism using different pipes and clips. Two (2) types of clips and four (4) types of pipes were tested (Figure 2, Table 1). In particular, a steel pipe (a) was used to define the extreme case of an absolutely rigid pipe. As a more realistic approach, the release mechanism with “flexible” pipes had to be investigated. Mechanisms with an easy-to-bend spiral plastic pipe (b) and a flexible pipe (c) were also tested. In these three cases the clip A with diameter $D=25\text{mm}$ was used. In an attempt to define the crucial parameters of the operation of the release mechanism, a system with a rusty rigid pipe (d) was also examined. In this test, the clip B with diameter $D=30\text{ mm}$ was used.

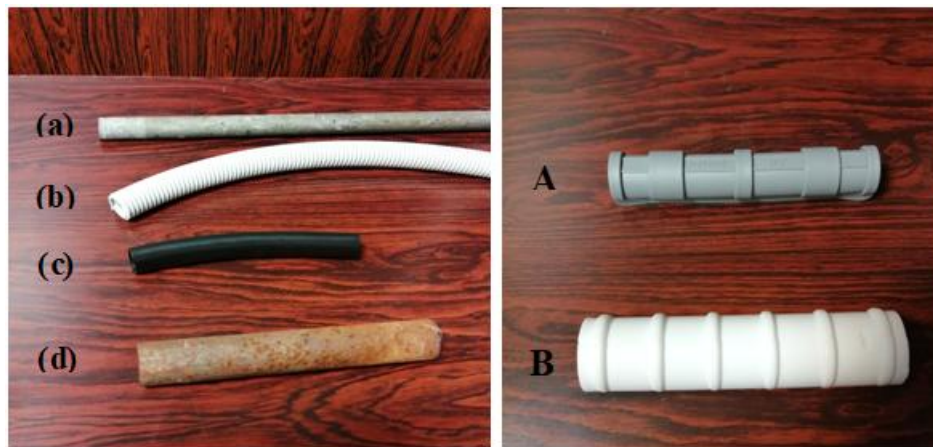


Figure 2. Experimental pipes and clips

Table 1. The components used for the different release mechanism configurations

<i>Experimental pipes</i>			<i>Experimental clips</i>
(a)	Rigid steel pipe	D=25mm	A
(b)	Spiral plastic Pipe	D=25mm	Plastic commercial Clip
(c)	Flexible plastic Pipe	D=25mm	D=25mm
			B
(d)	Rusty rigid Pipe	D=30mm	Plastic commercial Clip
			D=30mm

Preliminary experiments were carried out to determine the functionality of the mechanism. The impact of significant parameters such as the flexibility of the pipe and the stiffness of the clip on the procedure, should be clarified. The experimental setup for the series of the tensile tests is presented in Figure . Two insect-proof net samples of width equal to 100mm, were adjusted between the clip and the pipe to represent the integrated release mechanism configuration. The net samples width was chosen to be smaller than the clip width, while being adequately long, in order to allow for the proper operation of the mechanism and to simulate its presence on a nethouse structure. The net samples were fixed to the lower and upper clamp of the Instron device.

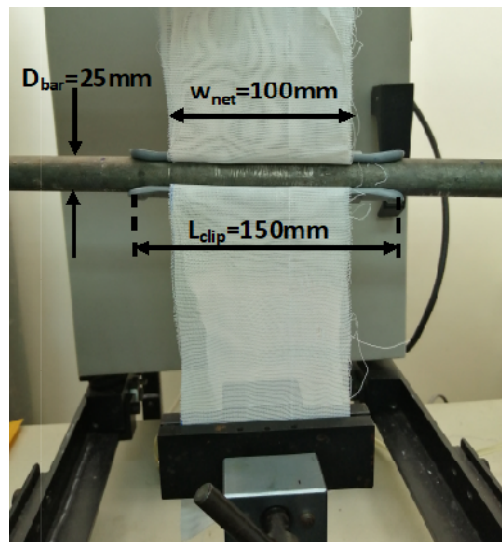


Figure 3.The experimental setup

The loading process was performed four times for each pipe (rigid, spiral, flexible, rusty rigid). It is very important to define the maximum load P [N] that depicts the load threshold that the release mechanism is activated at. The stress-strain curves of the tensile tests of the release mechanism with a rigid steel pipe and spiral pipe and Clip A appeared to be consistent, as presented in Figure and Figure 5. Both test cases had an elastic response and thus it was possible to load and unload without any kind of inelastic deformation at the components of the mechanism.

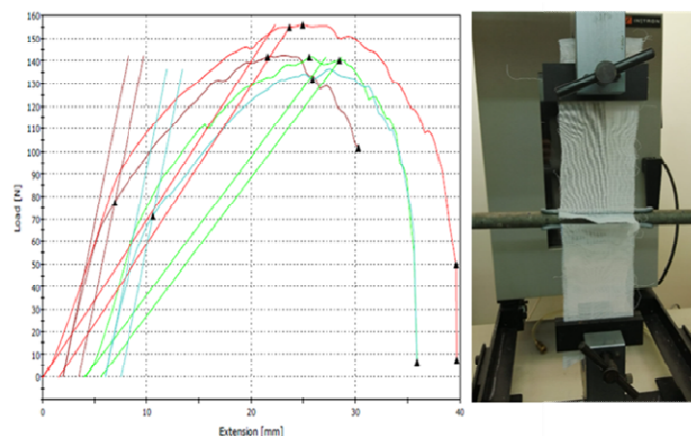


Figure 4.Stress-strain curves of the release mechanism with a rigid steel pipe and the corresponding laboratory test

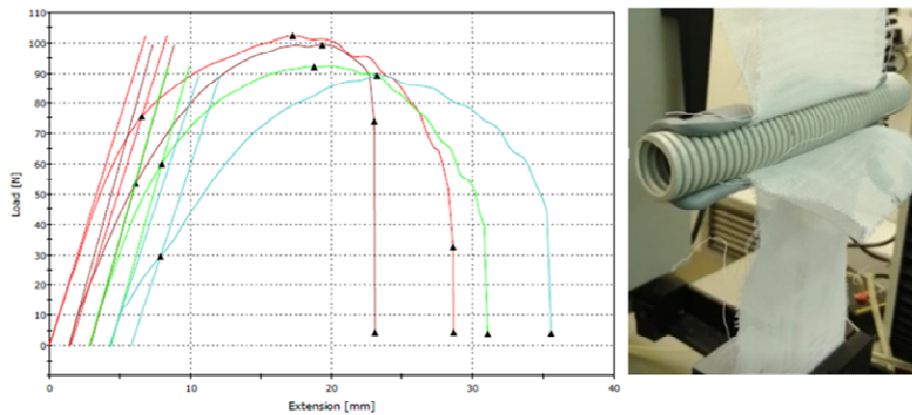


Figure 5. Stress-strain curves of the release mechanism with a spiral plastic pipe and the corresponding laboratory test

It was observed that the limit load, in the case of the steel pipe was higher than the case of the spiral pipe. The mean maximum limit load of all loading processes with an absolutely rigid steel pipe was equal to $P_{\max, \text{mean}}=143.5$ N. While in the case of the spiral pipe the maximum mean limit load was $P_{\max, \text{mean}}=95.5$ N. This outcome was rational, because the section of the spiral pipe was easier to bend perpendicular to the nets (in comparison to the rigid steel pipe) as the load increased. Bending of the pipe led to the unfastening of the mechanism components.

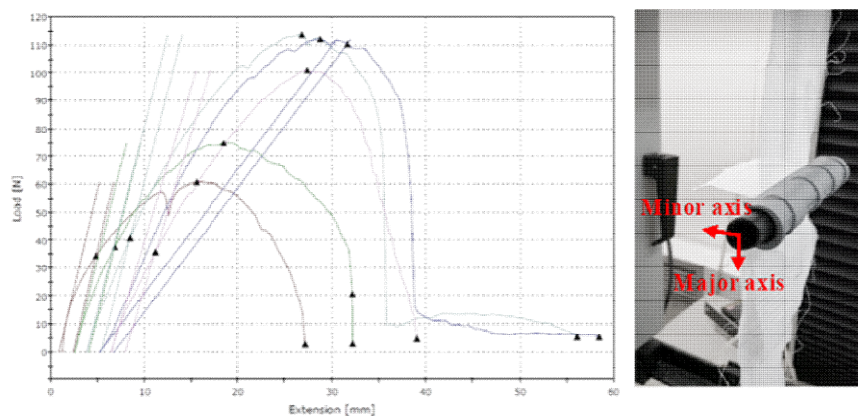


Figure 6. Stress-strain curves of the release mechanism with a flexible plastic pipe and the corresponding laboratory test

On the other hand, for the flexible pipe and Clip A configuration case, the stress-strain curves (Figure) lacked consistency and showed significant deviation regarding the limit load. The maximum limit load was $P_{\max}=113$ N and the minimum $P_{\min}=60$ N. This specific pipe exhibited elliptically shaped deformations of its cross sections after the initial test, obtaining

this way a cross-section of a major and a minor axis (Figure). It was found that attaching the pipe with each of axes inside the clip resulted in different values of the release load. For the pipe attached with the minor axis perpendicular to the nets, the release load was lower, since it was easier to slip and unfasten from the clip. On the other hand, the release load increased for the case where the major axis was perpendicular to the net sample.

In Figure the stress-strain curves of the tensile tests of the release mechanism with the rusty steel pipe and Clip B are presented. Results for this case showed that the capacity load further increased. The mean maximum limit load of the release mechanism with a rusty steel pipe was equal to $P_{\max, \text{mean}}=184$ N. This may be due to the different diameter of the pipe or even due to the friction between the components. This configuration could not be a proposed solution but an extreme example of understanding the influence of the involved parameter. The mean maximum loads of each experimental setup are provided in

Table 2.

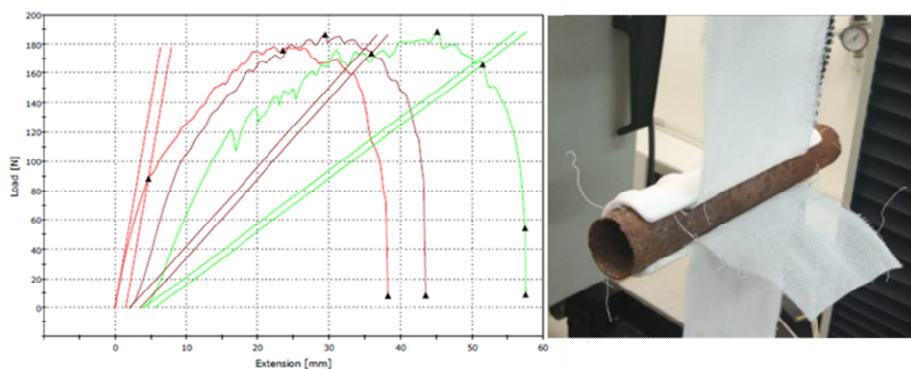


Figure 7. Stress-strain curves of the release mechanism with a rusty steel pipe and the corresponding laboratory test

Table 2. Mean maximum loads for different release mechanism configurations

<i>Experimental pipes</i>	<i>Mean maximum loads [N]</i>
(a) Rigid Steel Pipe	143.5
(b) Spiral Plastic Pipe	95.5
(c) Flexible Plastic Pipe	92
Rusty Steel Pipe	184

The preliminary experiments were performed to understand the pre- and post-release structural behavior and to investigate the load capacity of the various release mechanisms. Regarding the mean maximum load values, the highest value observed was equal to 184 N for the extreme case of the rusty steel pipe and the lowest equal to 92 N for the case of the flexible plastic pipe. Both aforementioned capacities seem to be relatively low. The use of stiffer components such as a steel pipe, showed increased load capacity for the mechanisms but not to a sufficient level. However, in order to increase the load capacity of the mechanism, the plastic clips could be reinforced locally using special steel components at specific distances. The special components can be made of steel to achieve higher capacities by designing the appropriate thickness of the component (Figure).



Figure 8.The steel components reinforces the clip

The subject of the ongoing research is the development of an improved methodology to design systems able to control the overloading by a release mechanism at specific predefined positions of the structure. The investigation of the static behavior of the mechanism will include the final structural and product design of the components of the release mechanism. Parameters like the thickness, the material, the shape and the position of the mechanism are some parameters the effect of which will be investigated in order to optimize the design of the incorporated release mechanism. The exact release load, the connectivity of the mechanism to the structure and the final product design (thickness, material, shape, etc.) is selected and designed based on the specific needs and requirements of each individual nethouse.